A multiscale time-Laplace method to extract relaxation times from non-stationary dynamic light scattering signals

François. Liénard, Éric. Freyssingeas, Pierre. Borgnat

A multiscale Time-Laplace method to extract relaxation times from non-stationary Dynamic Light Scattering signals

F. Liénard,[1] E. Freyssingeas,[1] and P. Borgnat[1]
ENS de Lyon, CNRS, Laboratoire de Physique, 69342 Lyon

(*Electronic mail: francois.lienard@ens-lyon.fr, eric.freyssingeas@ens-lyon.fr, pierre.borgnat@ens-lyon.fr)

(Dated: 17 November 2022)

Dynamic Light Scattering (DLS) is a well-known technique to study the relaxation times of systems at equilibrium. In many soft matter systems, we actually have to consider non-equilibrium or non-stationary situations. We discuss here the principles, the signal processing techniques we developed, based on regularized inverse Laplace transform, sliding with time, as well as the light scattering signal acquisition, that enable us to use DLS experiments in this general situation. In this article we show how to obtain such a Time-Laplace analysis. We claim that this method can be adapted to numerous DLS experiments dealing with non-equilibrium systems so as to extract the non-stationary distribution of relaxation times. To prove that, we test this Time-Laplace method on three different non-equilibrium processes or systems investigated by means of DLS technique: the cooling kinetics of a colloidal particle solution; the sol-gel transition; and the internal dynamics of a living cell nucleus.

I. INTRODUCTION

Dynamic light scattering (DLS), also known as Quasi-Elastic Light Scattering (QELS) or Photon Counting Spectroscopy (PCS), is a non-invasive spectroscopic analysis technique. Its fields of applications are diverse and range from chemistry, through biophysics, to physics. DLS principle is based upon analysis of the temporal fluctuations in the light intensity scattered by the sample under investigation, $I_{\text{scat}}(t)$.

One of the main applications of DLS is likely to be the size measurement of nano- and micro-scale particles in solutions, *e.g.* colloidal particles, micelles, polymers, proteins; all objects with radii smaller than $\sim 300\,\text{nm}$[1–3]. In this case, experiments are carried out with dilute solutions in stationary conditions so as to probe the Brownian motion of these objects. Nevertheless, particle sizing is not the only application of DLS. Several phenomena in statistical and soft condensed matter physics can be investigated thanks to DLS measurements: dynamics of liquid crystal phases[4–8], dispersions of colloids[9–11], micelles[12–14], polymers[15–18]. DLS measurements then are performed with more concentrated solutions and provide information on the collective relaxation processes, therefore, on the sample thermodynamics.

For all these reasons, DLS has been extensively used to probe the dynamics of "soft matter systems" in thermodynamic equilibrium for more than fifty years. To characterize the dynamics of the sample, commercial DLS devices return the autocorrelation function of the scattered light intensity, namely $g_2(\tau) = \langle I_{\text{scat}}(t) I_{\text{scat}}(t+\tau)\rangle$. The decay of $g_2(\tau)$ as a function of the delay τ is related to the relaxation times ζ_i (possibly several of them, hence the index i) of the sample. This technique allows to probe relaxation times of the system over a broad range, typically from microsecond to minute. In usual DLS applications, the investigated samples are in thermodynamic equilibrium, or at least stationary over the duration of the measurement.

Of course non-equilibrium or non-stationary systems scatter light as well, and therefore it is tempting to use DLS experiments to probe their dynamics. This has already been done for the study of continuous phase transitions[19,20], spinodal decomposition[21–23], as well as the dynamics of gels[24–28], glassy systems[29–32], or nucleus of a living cell[33–35]. However, in these cases, usual analyses of $I_{\text{scat}}(t)$ data no longer hold; particularly the autocorrelation function $g_2(\tau)$ of the scattered intensity only makes sense if the dynamics of the investigated system is stationary over the duration of its measurement. Theoretical models linking measurements of $g_2(\tau)$ to ζ_i assume, indeed, that the system is stationary. Here, as this is not the case, the computed autocorrelation function should depend on the time t at which it is estimated; that is: $g_2(\tau,t)$ instead of $g_2(\tau)$. The relaxation times of the sample, ζ_i, as well as the mean scattered intensity, evolve throughout the measurement. The signal measured in non-stationary DLS is thereby complex, and the analysis of its autocorrelation function is intrinsically complicated. The non-stationarity of $I_{\text{scat}}(t)$ may also appear as a long relaxation time (possibly longer than the typical duration T_0 on which autocorrelation is estimated). And mostly, an issue is how to deal with change in ζ_i with time during the acquisition. Consequently, to take full advantage of DLS technique to investigate the dynamics of non-equilibrium, non-ergodic or non-stationary systems, it is necessary to develop new signal processing methods able to reliably extract the time-dependent dynamics of these systems. The following properties are required:

- The analysis must be possible under non-stationary conditions. This means that the analysis has to be made time-dependent so that it evolves with t, the time at which it is carried out. Hence, formally, we have to work with a non-stationary autocorrelation function, $g_2(\tau,t)$.
- The duration of the data acquisition ΔT has to be taken into account, as well as T_0 the duration over which the autocorrelation function is estimated. Indeed, if ΔT is large compared to the time evolution of the ζ_i's, autocorrelation function will tend to provide time-average values, which poorly reflects the evolution of the system (especially for the short ζ). Conversely, if it is chosen a too short ΔT, it will no longer be possible to probe the

long relaxation time, even if they are stationary. Moreover, the measured $g_2(\tau,t)$ might be very noisy which will prevent good estimation even of the short ζ_i. So, it is required to adapt the estimation and choose a suitable T_0 which may vary and be different from ΔT.

- In out-of-equilibrium systems, there are often several characteristic relaxation times, denoted ζ_i, for $i = 1,...,M$, which occur at the same moment and that may be distributed over a broad time range. M is unknown, so is the time range, yet it is needed to find out all these times.

All that calls for developing a new methodology for the analysis of DLS data recorded on non-equilibrium, non-ergodic or non-stationary systems. This is the first objective of the present article. For this purpose, we will revisit S.W. Provencher's regularized Inverse Laplace Transform method[36,37], and from there develop an original Inverse Laplace Transform method that can be used as a multiscale, non-stationary method for DLS analysis. Thereby, the novelty of this work is to develop a comprehensive method for estimating a non-stationary inverse (and regularized) Laplace Tranform, which can cope the three issues mentioned above. Thus, the originality of the present work is to carefully study sampling, resolution, duration of the estimation window T_0, then to validate the method on various systems of soft matter.

Section II recalls in A the basics of DLS experiments, in B the classical analysis of DLS signals on systems in thermodynamic equilibrium, in C the attempts done to analyse DLS signals on non-stationary systems, finally in D we explain the aim of the present work and how we adapt the current analysis of DLS signals to non-stationary signals. Then, Section III describes the inverse Laplace transform procedure, based on the CONTIN method[36,37], which we develop to extract valuable information from non-stationary DLS signals. In the second part of this section it is discussed a numerical experiment validating this method. Next, in Section IV, it is first explained the proposed Time-Laplace approach that aims at following the time evolution of the relaxation times for non-equilibrium systems thanks to DLS experiments. Then it is described the experimental setting for data acquisition of the scattering signal required to allows this approach. Finally, in Section V in order to validate this method it is shown its application to the investigation of the dynamics of three different non-equilibrium processes or systems: the cooling kinetics of a colloidal particle solution; the sol-gel transition; and the internal dynamics of a living cell nucleus.

II. PRINCIPLES OF DYNAMIC LIGHT SCATTERING EXPERIMENTS AND THEIR ANALYSIS

Here, it is important to state that although the methods developed in this article can most likely be applied to heterodyne light scattering, cross-correlation light scattering, scattering wave spectroscopy (DWS) and X-ray photon correlation spectroscopy (XPCS), since the scattered intensity can be recorded continuously and an autocorrelation function (ACF) of the scattered intensity can be computed, in this article we only focus on the case of a single scattering process in a homodyne light scattering experiment.

A. DLS principles

Light scattering originates in the spatio-temporal fluctuations of the medium refractive index[38]. It therefore arises from the local optical properties of the sample, which are themselves linked to both the structure and the internal dynamics of the investigated sample. Fluctuations of the medium refractive index imprints information about particle motion in the scattering signal. We restrict the present study to light scattering in the Rayleigh-Gans-Debye regime (RGD). This theory is an approximate solution to light scattering by optically "soft" particles dispersed in a medium. Optical softness means that the size of particles is smaller or of the order of the light wavelength λ, and their refractive index n_1 is close to that of the surrounding medium n_0. The approximation holds for particles of arbitrary shape that are relatively small but may be larger than Rayleigh scattering limits; the RGD approximation implies: $a|n_0 - n_1|2\pi/\lambda \ll 1$, a being the size of the particles. In this framework, the refractive index of the medium can be written as a function of space $\vec{r}$ and time t, as: $n(\vec{r},t) = \langle n\rangle + \delta n(\vec{r},t)$, where $\delta n(\vec{r},t)$ represents both spatial and time fluctuations in the refractive index of the sample around its mean value $\langle n\rangle$; in most cases $\langle n\rangle \approx n_0$. The scattered electromagnetic field, E_{scat}, is proportional to the spatial Fourier transform of the fluctuations of $n(\vec{r},t)$, *i.e.* $\delta\hat{n}(\vec{q},t)$, where $\vec{q}$ is the scattering wave vector. Thereby, the scattered light intensity, $I_{\text{scat}}(q,t) = |E_{\text{scat}}(q,t)|^2 = E^*_{\text{scat}}(q,t)E_{\text{scat}}(q,t)$, is the "diffraction pattern" of the scattering volume (the sample's volume where the scattered light comes from). The size of the scattering volume is defined both by the optics and by the size of the hole placed in front of the detector.

For systems in thermodynamic equilibrium, the measured light scattering signal shows random fluctuations around a mean value: $I_{\text{scat}}(t) = I_0 + \delta I(t)$, with $\langle \delta I(t)\rangle = 0$. According to the RGD theory, these fluctuations are related to the dynamics of the processes involved in the temporal fluctuations of the refractive index n. For dispersions, these fluctuations $\delta I(t)$ come from the particle motion and reflect the randomly changing relative position of the particles as a result of thermal agitation. Thus analysis of $\delta I(t)$ yields information about the dynamics of the system. In the case of non-interacting particles (*i.e.* in practice for dilute samples) this provides information on the Brownian motion of the particles; henceforth DLS measurements give access to the diffusion coefficient of the objects: $D_0 = k_B T/6\pi\eta R_h$, where η is the solvent viscosity and R_h the hydrodynamic radius of the objects. In the case of interacting particles, then DLS measurements yield information on the thermodynamics of the system as well as on hydrodynamic interactions[39].

The principle of DLS experiment is therefore simple, as sketched on Fig. 1. It consists in passing a light beam (usually a laser beam of wavelength λ in its fundamental mode)

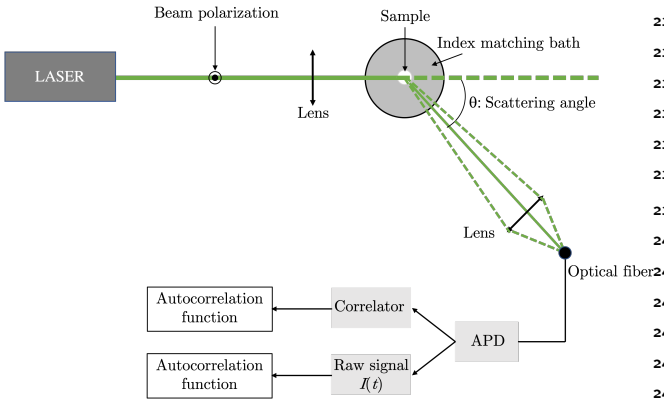

FIG. 1. Schematic representation of DLS set-up.

through the sample, and to study the light intensity scattered by the sample in a given direction. The scattered light intensity, $I_{\text{scat}}(\vec{q},t)$ coming from the scattering volume, is detected by means of a photodetector placed at an angle θ with respect to the incident laser beam direction. This angle selects the scattering wave vector $\vec{q}$, the module of which is given as a function of the mean refractive index $\langle n\rangle$ of the dispersion and the incident light wavelength λ:

$$q = \left(4\pi\langle n\rangle \sin(\theta/2)\right)/\lambda. \tag{1}$$

This scattering wave vector sets the length scale l over which light scattering probes the fluctuations of the refractive index n: $l \approx 2\pi/q$. By varying the scattering angle θ, q is varied, thus allowing for probing the sample dynamics over spatial scales ranging from hundreds of nanometers ($\sim \lambda/2\langle n\rangle$) to a few micrometers.

B. Classical methods for analyses of stationary DLS signals

The starting point for analyzing temporal fluctuations of the scattered light intensity is the estimation of its ACF $g_2(\tau)$. In general, the incoming data are processed in real time using a digital signal processing device known as a correlator that outputs an estimate of the ACF of the scattered intensity as a function of the delay time τ. This ACF, $g_2(q,\tau)$ is written:

$$g_2(q,\tau) = \langle I_{\text{scat}}(-q,t) I_{\text{scat}}(q,t+\tau)\rangle \tag{2}$$

Note that here, the explicit dependence on q has been taken into account in order to relate the measured ACF to I_{scat} and E_{scat}. This latter equation can also be expressed as

$$g_2(q,\tau) = \langle I_{\text{scat}}(q,t)\rangle^2 \left(1+\beta|g_1(q,\tau)|^2\right) \tag{3}$$

This equation is known as the Siegert relation[38] $\langle I_{\text{scat}}(q,t)\rangle = I_{\text{scat}}(q)$, is the static scattering intensity at wave vector $\vec{q}$; $g_1(q,\tau)$ is the first-order ACF, defined as: $g_1(q,\tau) = \langle E^*_{\text{scat}}(q,t) E_{\text{scat}}(q,t+\tau)\rangle$, hence $g_1(q,\tau) \propto \langle \delta\hat{n}(-q,t)\delta\hat{n}(q,t+\tau)\rangle$. The factor β is the inverse of the number of coherence area on the photodetector surface, *i.e.* the number of speckle spots; $0 \leq \beta \leq 1$.

Note that in the rest of this article, we get rid of the dependence on q; both for reasons of simplicity, and also because in the following it is only considered experiments with fixed q; hence we write: $g_2(\tau) = \langle I_{\text{scat}}(t)\rangle^2 \left(1+\beta|g_1(\tau)|^2\right)$, with $g_1(\tau) \propto \langle \delta\hat{n}(t)\delta\hat{n}(t+\tau)\rangle$.

The first step of a DLS experiment is to obtain an ACF $g_2(\tau)$ that can be readily analyzed. To obtain such a function care must be taken. If T_0 is the duration over which the ACF of the scattered intensity is computed, the scattering signal has to be stationary over T_0, *i.e.* $\langle I_{\text{scat}}(q,u)\rangle = \text{cste}, \forall u \in [0,T_0]$. The largest value of the probed τ has to be larger than the slowest relaxation time of the system; and T_0 must be, at least, 10 times larger than the last value of the probed τ. If all that is satisfied, then $g_2(\tau)$ could be correctly estimated. Moreover, noise may be reduced by iterating the computation of $g_2(\tau)$ to average them. In such cases, it provides accurate information on the dynamics of systems in thermodynamic equilibrium, or at least in a stationary state throughout the experiment duration. (Note that using a correlator, T_0 and the signal duration acquisition ΔT are always identical. However, if the ACF is computed from the measurement of $I_{\text{scat}}(t)$, T_0 can be different from ΔT). If it is used a correlator that typically probes τ between 10^{-8} s and 1000 s, (their optimal operating range, in practice, is rather 10^{-6} s - 10 s), this first step works well for systems the relaxation times of which are included within this latter range that corresponds to most of "soft matter" systems in thermodynamic equilibrium.

The second step of a DLS experiment is to extract the relaxation times ζ_i of the investigated sample from the measured ACF $g_2(\tau)$. The objective is, on the basis of physically relevant characteristics of the probed system, to relate $|g_1(\tau)|^2$ to the relaxation times. For example, in the canonical case of a dilute solution of monodisperse nanospheres, there is only a single relaxation time ζ related to the Brownian diffusion of the particles. Thereby $|g_1(\tau)|^2 = \mathrm{e}^{-2\tau/\zeta}$, where: $1/\zeta = D_0 q^2$, D_0 being the diffusion coefficient of the spheres, *i.e.* $D_0 = k_B T/6\pi\eta R_h$ as recalled above. Using a parametric fit $\left(g_2(\tau) = A + B\mathrm{e}^{-2\tau/\zeta}\right)$, it is easy to obtain ζ, and then the hydrodynamic radius of the particles. Actually, particles are often polydisperse and then $|g_1(\tau)|^2$ is no longer a simple decaying exponential function. For slightly polydisperse spheres, the ACF can then be fitted to a cumulant expansion around some mean relaxation time ζ: $|g_1(\tau)|^2 \simeq \mathrm{e}^{-2\tau/\zeta}\left(1+\mu_2\tau^2/2+\ldots\right)^2$, where μ_2 is the 2nd order moment of the particle size distribution; and this parametric expansion can be continued to higher orders[40–42]. However, this method is only adapted to systems that exhibit a single polydisperse relaxation time.

Unfortunately, not all the systems are as simple as slightly polydisperse nanospheres in dilute solution. Still, many methods have been proposed to fit (either linearly or non-linearly) $|g_1(\tau)|^2$ in terms of the cumulants (or moments) of the relaxation times distribution[41–44]. However many systems are actually much more complex. They can, indeed, exhibit several relaxation times that can be broadly distributed over many

decades, with in some cases very long relaxation times, larger than a few seconds[4–18]. Under these conditions, one approach is to fit $|g_1(\tau)|^2$ to a model that is the square of a sum of exponential decays. Thus:

$$|g_1(\tau)|^2 = \left| \sum_{i=1}^{M} a_i \, \mathrm{e}^{-\tau/\zeta_i} \right|^2 \qquad (4)$$

with $M > 2$ the number of modes, and ζ_i the mean relaxation time of the i^{th} process. It can even be used a more complicated model, where it is assumed a time relaxation polydispersity around each ζ_i (as in the previous model). Nonetheless, these approaches fail quickly due to the large number of fitting parameters required. Often, in complex cases, to take into account several relaxation times, $|g_1(\tau)|^2$ is modeled by the empirical Kohlrausch-William-Watts (KWW) form[6,43,45]: $|g_1(\tau)|^2 = \mathrm{e}^{-2(\tau/\zeta)^{\alpha}}$, where α is a parameter, which in the case of systems in equilibrium is in the range $[0,1]$. Then $g_1(\tau)$ is a stretched exponential function, which means that it decays slower than a single exponential relaxation. This is assumed to reflect the existence of a broad distribution of relaxation times. However, even if this kind of functions fits to $|g_1(\tau)|^2$ properly, physical interpretation of both ζ and α may be difficult. Moreover, as it was stated by Madsen *et al.*[46] and Andrews *et al.*[43,44], KWW models do not always capture the whole relaxation processes present in the ACF.

Henceforth, in the general setting, and especially for systems with a broad distribution of relaxation times, a good approach to interpret DLS measurements is to move to a non-parametric method and to consider that $g_1(\tau)$ provides the Laplace transform (LT) of a density distribution of relaxation times, $G(s)$:

$$g_1(\tau) = \int_0^{+\infty} G(s) \, \mathrm{e}^{-\tau/s} \, \mathrm{d}s \qquad (5)$$

Eq. (5) is the Laplace transform of G, except that here the Laplace variable s has the same dimension as τ. Note that in this article, we use s for the Laplace variable and keep a distinct notation ζ for the relaxation times.

Hence, as already advocated by S. Provencher[36,37], and also more recently by Andrews *et al.*[43,44], rather than a parametric fit, to get all the relaxation times ζ_i, it is more powerful to estimate the inverse Laplace transform (ILT) of $g_1(\tau)$. Therefore, to obtain a non-parametric estimation of $G(s)$, one has simply to invert eq. (5). The difficulty is that the ILT process is numerically an ill-conditioned problem, prone to be very sensitive to any experimental or numerical noise. In references[36,37], it is developed a method for regularized inverse Laplace transform, called CONTIN that is particularly used in the analysis of DLS and X-ray photon correlation spectroscopy (XPCS) autocorrelation functions (its applications, however, are much broader than just these fields). The major contribution of S. Provencher[36,37] was to develop and validate, both mathematically and numerically, an algorithm to compute the ILT of the ACF in a stable manner thanks to a regularization of this ill-conditioned problem. Many different solutions for ILT have been developed with other approaches including maximum entropy[47], maximum likelihood[48] or non-negative SVD[49]. Compared to parametric fits or other methods, the CONTIN method requires little prior knowledge about the relaxation times of the investigated system. Note that this approach works for both ACFs built using a correlator and ACFs computed from $I_{\mathrm{scat}}(t)$. (*For particle sizing, the CONTIN method is now a routine analysis used in commercial DLS softwares.*)

C. Current approaches for non-stationary DLS signals.

In principle, for experiments on non-equilibrium or non-stationary systems, the approaches described in the former section should not be employed. Nonetheless, because of the interest of DLS or XPCS techniques to probe the dynamics of Soft Matter, works have used these techniques to investigate non-equilibrium systems. Therefore, many attempts were made to follow the temporal evolution of non-stationary scattered signals. Time-resolved-correlation measurements were proposed to quantify statistically dynamical heterogeneities[50,51]. Two-time correlation functions were used to represent the temporal evolution of ACFs in two dimensions[46,52–54]. All these works are very interesting and in these cases, the authors overcame to extract relevant information on the dynamics of the investigated systems.

Fluerasu *et al.*[52], Madsen *et al.*[46,55] and Cipilletti *et al.*[56] investigated dynamics of gels or glassy-like systems by analysing the ACFs of the scattered intensity using KWW models. Mostly, they followed the temporal evolution of the coefficient α of the KWW model. In these cases, and contrary to what is observed for systems at thermodynamic equilibrium, it can be found $\alpha < 1$, or $\alpha > 1$. Sometimes, as for equilibrium systems, the ACF is a stretched exponential, and then α is likely the signature of a broad distribution of relaxation times. But at other times, it is found $1 < \alpha$; when $1 < \alpha$, $g_1(\tau)$ is a compressed exponential function, which means the ACF decays faster than a single exponential relaxation. The physical meaning of such a relaxation is not yet well understood. Nevertheless, such approaches allow to characterise the investigated dynamics through the degree of stretching or compression of its exponential relaxation. For aging systems slow dynamics can be investigated thanks to such methods, yet assumptions on the dynamics are required and faster relaxations are overlooked, or not investigated, as mentioned[43,46]. All these analyses manage to provide temporal evolution of an average behavior of the dynamics as well as of its heterogeneities. These analyses, however, do not attempt to measure the relaxation spectrum, *i.e.* the different characteristic times that compose the dynamics of the investigated systems, nor their evolution as a function of time.

It is still lacking an accurate signal processing tool able to quantify, from DLS measurements (or XPCS), the whole dynamics of a non-stationary system as a function of time (at least over a broad range of relaxation times). Indeed, from our knowledge, there is no systematic, multiscale and free-of-a-priori method available yet to analyse non-stationary signals of DLS in order to obtain the full spectrum of relaxation

times of an out-of-equilibrium system and follows its evolution. This is the goal of our article.

D. Adaptation of "CONTIN" based methods to non-stationary signals.

In this article, we intend to bring about a general, systematic and accurate method allowing to extract temporal evolution of the relaxation times of non-stationary signals. As we aim to investigate samples having, *a priori*, a dynamic with many relaxation times, polydispersed and spread over a broad time range, we believe that the best approach is to assume that the ACF of the scattered intensity is the Laplace transform of a density distribution of relaxation times. In this case, however, the ACF is a non-stationary function of the time t and, consequently, one should deal with a more general non-stationary ACF, which is $g_2(\tau,t,T_0)$, and the corresponding $|g_1(\tau,t,T_0)|^2$. There, indeed, the ensemble average is replaced by a local temporal average computed between t and $t+T_0$, where T_0 is the duration over which the ACF is built. In this notation, we highlight the dependence of $g_2(\tau)$ with t, which is the starting time of the ACF measurement. Furthermore, we make explicit that the estimation of $g_2(\tau,t,T_0)$ (*i.e.* $g_1(\tau,t,T_0)$), also depends on the duration over which $g_2(\tau,t)$ ($g_1(\tau,t)$) is computed. Therefore, $g_1(\tau,t,T_0)$ can be written as the Laplace transform of a density distribution of relaxation times, $G(s,t,T_0)$:

$$g_1(\tau,t,T_0) = \int_0^{+\infty} G(s,t,T_0)\,\mathrm{e}^{-\tau/s}\,\mathrm{d}s \qquad (6)$$

Let us explain the ideas behind our approach. First of all, it is chosen a first starting time t_1, and $g_1(\tau,t_1,T_0)$ is computed between t_1 and t_1+T_0. Then, it is chosen a second starting time t_2, and a new ACF $g_1(\tau,t_2,T_0)$ is computed between t_2 and t_2+T_0. This process is iterated in order to achieve a series of ACFs whose starting times are all different. Thanks to eq (6), each of these $g_1(\tau,t_i,T_0)$ is related to a density distribution of relaxation times $G(s,t_i,T_0)$. As in the classical CONTIN used on systems in equilibrium, here also one has to invert eq. (6) to obtain a non-parametric estimation of the distribution of relaxation times $G(s,t_i,T_0)$. Such a procedure should provide the relaxation times of the studied system as a function of time; *i.e.* $\zeta_j(t_i)$. This use of a sliding window connects the method to a non-stationary setting. T_0 reminds us that $G(s,t_i,T_0)$ (and thus the relaxation times ζ_j), cannot be well estimated when they are not small enough compared to T_0. Hence, by playing with T_0, it is possible to change the investigated s range, allowing thus a multiscale approach of the scattering signal analysis.

In order to follow such a strategy to investigate the dynamics, as well as its time evolution, for non-equilibrium and non-stationary systems, care has to be taken when measuring $g_2(\tau,t,T_0)$. It is obvious that building the ACF of the scattered intensity thanks to a correlator will not bring about worthwhile results, since the correlator returns $g_2(\tau,t,\Delta T)$, where t can not be tuned. A direct measurement of the scattered intensity $I_{\mathrm{scat}}(t)$, with a high acquisition rate and over a long period of time Δt, is indeed necessary to apply our signal processing. Once $I_{\mathrm{scat}}(t)$ recorded, the different $g_2(\tau,t_i,T_0)$ ($g_1(\tau,t,T_0)$) can be computed, where it will be possible to play with both parameters t_i and T_0 in order to be able to finely follow the time evolution of the dynamics (multi scale approach). As written previously, to analyze these functions properly, the first step of this work is, therefore, to rewrite a new version of CONTIN that takes into account a logarithmic distribution of the delay times τ, over at least $6-7$ decades, with appropriate regularization that makes it resilient to experimental noise and statistical limits in the estimates of ACFs over these broad time ranges. We will then demonstrate that this modified version of CONTIN is still a suitable non-parametric method to allow, from DLS measurements, the extraction of characteristic relaxation times of systems with multiple relaxation processes and high polydispersity. This modified algorithm, indeed, is a new ILT algorithm.

That is by combining computation of $g_1(\tau,t,T_0)$ functions, from $I_{\mathrm{scat}}(t)$ measurements, with the new ILT algorithm, that the time evolution of the dynamics of non-equilibrium and non-stationary systems can be accessed. This will be proved on experimental situations.

The objectives and novel contributions of the present article are the following:

- Revisit the classical CONTIN method in a modern and practical way, so as to put forward its advantages when processing non-stationary DLS experiments.
- Provide a "Time-Laplace method" that brings a systematic way to analyze the temporal evolution of relaxation times for systems exhibiting multiple relaxations and strong polydispersities.
- Provide a multiscale approach allowing to monitor the resolution of the relaxation times and of their evolution.

III. NON-STATIONARY DLS SIGNAL PROCESSING BASED ON INVERSE LAPLACE TRANSFORM

A. Log spaced and weighted Inverse Laplace Transform algorithm.

Let's assume that we have a measure of the scattered light intensity as a function of time, $I_{\mathrm{scat}}(t)$ (we will describe the procedure for acquiring $I_{\mathrm{scat}}(t)$ in section IV B). The starting point of the procedure we develop here is the estimation of the ACFs of the scattering intensity (**ACF**) from $I_{\mathrm{scat}}(t)$. Hereafter these estimated ACF are noted $\hat{g}_2(\tau,t,T_0)$. As discussed, these ACF are computed over a time window of length T_0, between time t and $t+T_0$. In practice, to probe a broad range of relaxation times, $\hat{g}_2(\tau,t,T_0)$ is calculated as a logarithmic downsampled version of the standard, biased and normalized, autocorrelation estimator, expressed with the centered intensity $I^c(u) = I_{\mathrm{scat}}(u) - \sum_{v=t}^{t+T_0} I(v)$. Therefore $\hat{g}_2(\tau,t,T_0)$ writes

as:

$$\hat{g}_2(\tau,t,T_0) = \frac{\sum_{u=t}^{t+T_0-\tau} I^c(u)I^c(u+\tau)}{\sum_{u=t}^{t+T_0} I^c(u)^2}. \quad (7)$$

Here $\hat{g}_2$ is normalized (on contrary to g_2 in eq. (3)). One can notice that this expression of $\hat{g}_2(\tau,t,T_0)$ is as writing that:

$$\hat{g}_2(\tau,t,T_0) = \frac{\langle I_{\text{scat}}(t)I_{\text{scat}}(t+\tau)\rangle_{T_0} - \langle I_{\text{scat}}(t)\rangle_{T_0}^2}{\langle I_{\text{scat}}(t)\rangle_{T_0}^2} \quad (8)$$

Which according to Siegert's equation (eq. (3)) is equivalent to

$$\hat{g}_2(\tau,t,T_0) = \frac{1}{\beta}\left(\frac{\langle I_{\text{scat}}(t)I_{\text{scat}}(t+\tau)\rangle_{T_0}}{\langle I_{\text{scat}}(t)\rangle_{T_0}^2} - 1\right) = |g_1((\tau,t,T_0)|^2 \quad (9)$$

The estimated ACF, $\hat{g}_2$, is thus equal to $|g_1|^2$. Hence, by normalizing and centering the ACF, the experimental aspects of the measurement are eliminated (the baseline and β) to give rise to a quantity directly related to g_1. Moreover, if one would assume a model as in eq. 4:

$$|g_1(\tau)|^2 = \left|\sum_i^M a_i \mathrm{e}^{-\tau/\zeta_i}\right|^2 = \sum_i |a_i|^2 \mathrm{e}^{-2\tau/\zeta_i} + \sum_{i\neq j} a_i a_j^* \mathrm{e}^{-\tau/\zeta_i - \tau/\zeta_j}, \quad (10)$$

then the cross terms are in fact negligible, or more precisely, incorporated in the broadening of the distributions as if there were some polydispersity. For example, if ζ_i and ζ_j are very different, then the cross term is dominated by the smaller one and it is inside the peak associated to it. On the other hand, if they are close to each other, $1/\zeta_i + 1/\zeta_j \simeq 2/\zeta_i$, and thus they are not distinguishable from polydispersity. Therefore

$$|g_1(\tau)|^2 \simeq \sum_i |b_i|^2 \mathrm{e}^{-2\tau/\zeta_i} \quad (11)$$

where the amplitudes b_i reflect the influence of the cross terms. Thereby

$$\hat{g}_2(\tau,t,T_0) \simeq \sum_i |b_i(t,T_0)|^2 \mathrm{e}^{-2\tau/\zeta_i(t,T_0)} \quad (12)$$

Hence one expect the characteristic (local) relaxation times of $\hat{g}_2(\tau)$ to be equal to the half of the ζ_i, and therefore the ILT of $\hat{g}_2(\tau)$, should provide relaxation times that are the half of the real relaxation times.

ILT algorithms, such as CONTIN, aim at performing the inverse Laplace transform of $\hat{g}_2(\tau)$, by numerically solving an inverse problem to provide an estimate $\hat{G}$ written as follows:

$$\hat{G}(s,t,T_0) = \arg\min_{G\in\mathscr{G}} \left(\|LT(G) - \hat{g}_2(\tau,t,T_0)\|_w^2 + \gamma^2 R(G)\right) \quad (13)$$

where $R(G)$ is the regularization term, γ a parameter, $\mathscr{G}$ is the set of constraints defining the admissible G, and $w(\tau)$ leaves the possibility to have a weight in the norm with respect to the delay τ. The discretization of the Laplace transform has to be specified, as well as the choice for the regularizations and weights. To take advantage of the acquisition of the scattered light intensity over a long duration, we use a logarithmic sampling both in the delays τ_j and in the Laplace variable s_k. This sampling goes from the smallest measured delay τ_1 (equal to the sampling interval) up to $\tau_N = T_0$, as it is the maximum value that makes sense. A similar sampling is done for the s_k, using N_s points. $LT(G)$ is computed as the discretized expression of the integral in eq. (6):

$$LT(G)(\tau_j) = \sum_{k=1}^{N_s} G(s_k)\mathrm{e}^{-\tau_j/s_k} \quad (14)$$

The set of constraints $\mathscr{G}$ is that $\forall s,\ G(s) \geq 0$. The regularization term $R(G)$ is taken to promote regularity and smoothness, with a minimum number of peaks; an adequate choice is $R(G) = \left\|D^{(2)}(G)\right\|^2$, where $D^{(2)}$ is the second order discrete difference operator, which writes:

$$D^{(2)}\left(G(s_k)\right) = G(s_{k+1}) - 2G(s_k) + G(s_{k-1}) \quad (15)$$

The weight function $w(\tau)$ is introduced in the first term of eq. (13) because it is expected, by letting the τ_j's increase up to T_0, to have higher statistical fluctuations at large delays than at small delays. This constrains $LT(\hat{G})$ to follow more closely $\hat{G}_2$ at short delays than for the large delays. This weight is:

$$w_j = w(\tau_j) = \sqrt{\frac{T_0}{\tau_j}} \quad (16)$$

Indeed, it can be expected that the variance of the fluctuations of the autocorrelation estimators[57] roughly evolves as τ/T_0. In other words, the number of decorrelated measures at delay τ over a duration T_0 evolves as T_0/τ and this leads to the following choice of weighting.

Altogether, and introducing both the logarithmic increments Δsk and $\Delta\tau_j$, as well as the matrix notation $(\mathbf{A})_{jk} = \exp(-\tau_j/s_k)$ for the exponential term in the LT, it is obtained the discrete form of the eq. (13):

$$\hat{G}(s,t,T_0) = \arg\min_{G\geq 0} \sum_{j=1}^{N} w_j \left[(\mathbf{A}G)_j - \hat{g}_2(\tau_j,t,T_0)\right]^2 \Delta\tau_j + \gamma^2 \sum_{k=1}^{N_s} \left[D^{(2)}\left(G(s_k)\right)\right]^2 \Delta s_k \quad (17)$$

where N is the size of the downsampled vector $\hat{g}_2$.

The minimization of eq. (17) is implemented in Matlab, based on the CONTIN algorithm[36,37] and adapted from the implementation of Marino[58]. It alternates between finding the minimum of the unconstrained problem with the simplex algorithm (using `fminsearch` in Matlab), and projecting over the constraint.

In the next section, we verify that the choices of ACF normalization, discretization, and weighting work properly in our implementation.

B. Numerical validation in stationary condition.

The first step is to prove that this method of analyzing ACFs works. There are several requirements to check its proper functioning. Obviously, this strategy has to be able to measure reasonable values for each of the relaxation times present in the ACF. Secondly, the ratio between two densities of relaxation times needs to be approximately preserved through the analysis. Thirdly, the regularization must work uniformly for the all ranges of relaxation times.

To test these three points, this method is first applied to modeled ACFs. For this purpose, ACFs described by a sum of decreasing exponential functions were modelled in which some polydispersity was incorporated as in the cumulant expansion model (here with order 2 in the cumulants only). These ACFs follow the model:

$$g_{2,\mathrm{mod}}(\tau) = \frac{\sum_{i=1}^{M} A_i \mathrm{e}^{-\tau/\zeta_i}\left(1+\frac{1}{2}\left(\sigma_i\tau/\zeta_i\right)^2\right)}{\sum_{i=1}^{M} A_i} \qquad (18)$$

where M is the number of relaxation modes; A_i is the amplitude of mode i, ζ_i its mean relaxation time, and σ_i the relative standard deviation associated to ζ_i (so that $\sigma_i^2 = \mu_{2i}\zeta_i^2$). Finally, it is added noise to these ACFs. As in the experiments, the noise is higher at long times than short ones. Then, the ILT algorithm we developed is applied to these ACFs to compute the density function of the relaxation times $\hat{G}(s)$. It is always observed a very good agreement between the modelled ACFs and $\hat{G}(s)$ calculated by means of the ILT algorithm that has been developed.

This numerical validation is illustrated with the following example. An ACF is modelled with 5 different relaxation times (*i.e.* $M = 5$), distributed over 8 decades in time, with for each relaxation time a polydispersity of 20% ($\forall i$, $\sigma_i = 0.2$). The five relaxation times ζ_i are: 10^{-5} s, 10^{-4} s, 10^{-3} s, 10^{-2} s, 10^{-1} s, respectively, with the following mode amplitudes: $A_i = 1, 0.2, 0.5, 1, 0.2$. This ACF is displayed in Fig. 2 (a); it is the orange dashed curve. Then, a random noise increasing with τ is added to this ACF to form a noisy ACF, which is also shown in Fig. 2 (a); that is the blue curve.

Then $\hat{G}(s)$ are calculated for both the noisy and the noise-free ACFs thanks to the ITL algorithm that was developed. The parameters that control the ILT algorithm are N, the number of points in τ used to sample the ACF, and N_s, the number of points in s used to sample $\hat{G}$. For this test, it is set $N = N_s = 100$, so as to cover well the time range from 3.10^{-8} s to 3 s, with logarithmic spacing; there are about 12 points per decade. The parameter γ of eq. (13) is the last parameter to be fixed, it is however the most delicate to choose. We will discuss it at the end of the subsection. Here, it is fixed at $\gamma = 0.1$. For comparison, the relaxation time distributions of these modelled ACFs are also estimated using the classical CONTIN algorithm (with the same parameters)), $\hat{G}_{direct}(s)$.

The calculated $\hat{G}(s)$ are displayed in Fig. 2 (b) and Fig. 2 (c), for the noisy and the noise-free ACFs, respectively (both gray solid lines). In both cases, five distinct peaks, well defined, are observed. The analysis of the noise-free ACF almost exactly returns the properties of this ACF. Let's now focus on the analysis of the noisy ACF. The peaks of relaxation times are obtained for: $\zeta_i \simeq 10^{-5}$ s, $9.4\,10^{-5}$ s, $1.1\,10^{-3}$ s, $9.9\,10^{-3}$ s, $1.1\,10^{-1}$ s, respectively. These values correspond to the inputs ζ_i's nearly perfectly. It is likely that this small difference lies in the grid discretization; checking closely, when the input value is comprised between two points of the logscale sampling, the measured value is always one of these two points. The measured amplitudes for the different modes are: $A_i \simeq$ 0.15, 0.034 ,0.072, 0.13, 0.030, respectively. One can note that ratios between amplitudes are almost preserved, even if the amplitudes are not. It can be noted, qualitatively, that the relative widths of the peaks are similar (*i.e.*, with respect to the relaxation times). For each peak, the standard deviation to relaxation time ratio is computed and it is found: $\hat{\sigma}_i = 17$, 14, 17, 18, 15 %. It remains some discrepancies with the set value, likely due to noise and numerical resolution, yet the result is satisfactory, demonstrating the uniformity of the regularization across s. Therefore, the used ILT algorithm perfectly captures the ACF features for the noisy ACF as for the noise-free ACF; this result demonstrates the robustness of our algorithm to noise.

In Fig. 2 (b) and Fig. 2 (c), it is also displayed $\hat{G}_{direct}(s)(s)$ estimated using a classical CONTIN algorithm, for the noisy and the noise-free ACFs, respectively (green dotted lines). This algorithm does not take into account the logarithmic scale specifically, nor the weight w. CONTIN algorithm allows to recover, roughly, the characteristics of the ACF. The result, however, is obviously not as good as that obtained by means of the ILT algorithm developed in this work. It is clearly seen that using CONTIN algorithm, the regularization is not uniform along the s-axis: one observes several peaks for long relaxation times whereas broad peaks are observed at short relaxation times. It is also noticed that the CONTIN algorithm does not correctly preserve homogeneity of the peaks width; in this case, it depends on the considered time range. These observations emphasize the necessity to take into account the logscale, as well as used a weight function to reduce the effect of noise on ILT process.

It is worth noticed that if one wishes to analyze this ACF using a parametric fit, then this would require a very large number of parameters. Indeed, if trying to fit a cumulant model to such an ACF, 15 different parameters are necessary. Moreover, this would require having prior knowledge on the number M of relaxation times. It is, therefore, unrealistic to expect that such a fit can correctly evaluate such ACFs.

As mentioned before, for the implementation of the ITL algorithm developed in this work, it remains the question of the choice of the parameter γ. In fact, as for the classical CONTIN algorithm. The precise estimation of this parameter is a challenge. A too low value of γ can lead to artifacts, as a single relaxation time with a slight polydispersity can be detected as multiple relaxation times. On the other hand, a high value of γ may excessively smooth the solution, resulting in non-discrimination between two close relaxation times, or overestimation of the polydispersity of the sample. To determine γ in a heuristic way, multimodal ACFs are simulated from eq. (18) in order to estimate the resolution of the method. Here we do not detail the protocol used, but

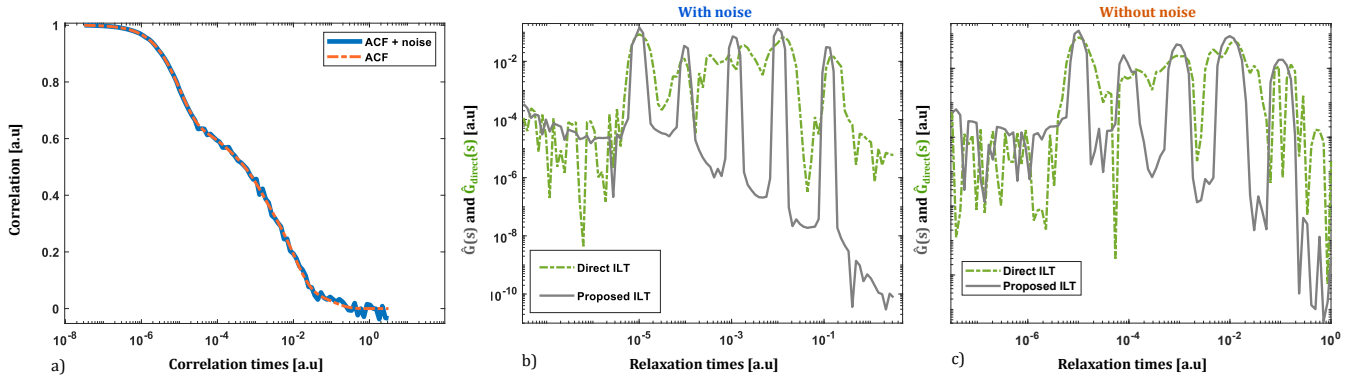

FIG. 2. Left panel (a): modeled ACF from eq. 18; $M = 5$, with $\zeta_i = 10^{-5}$ s, 10^{-4} s, 10^{-3} s, 10^{-2} s, 10^{-1} s, respectively, and $A_i = 1, 0.2, 0.5, 1, 0.2$. The polydispersity around each relaxation time is the same: ($\forall i$, $\sigma_i = 0.2$). The orange dashed line is the noise-free ACF; the blue solid line is the noisy ACF (a random noise increasing with τ was added to this ACF). Middle panel (b): density distributions of the relaxation times computed for the noisy ACF; using the ILT algorithm we developed ($\hat{G}(s)$; gray solid line), and a classical implementation of CONTIN[58] ($\hat{G}_{direct}(s)(s)$; green dashed line), this latter algorithm does not take into account weighting w nor a logarithmic scale, $\gamma = 0.1$ in both cases. Right panels (c): density distributions of the relaxation times computed for the noise-free ACF; using the ILT algorithm we developed ($\hat{G}(s)$; gray solid line), and a classical implementation of CONTIN[58] ($\hat{G}_{direct}(s)(s)$; green dashed line)

the idea behind this study is to set γ so that relaxation times separated by at least one decade are always discriminated, and that each peak with a polydispersity of the order of 25% is not split into several peaks. With such an idea, it found out that a good compromise is obtained when γ belongs the interval $[0.1 - 10]$. Usually, under these conditions, the relaxation times can be separated if there is at least a ratio of 3 between these times. These values of γ also imply that one cannot estimate a polydispersity lower than 10%; below this value, such a polydispersity will lead to a broadening of the peaks similar to the smoothing imposed by the regularization

IV. TIME-LAPLACE APPROACH FOR OUT-OF-EQUILIBRIUM SYSTEMS

There is now a ILT algorithm for extracting a large number of relaxation times, spread over a broad time range, from any measured $g_2(\tau,t,T_0)$ ($g_1(\tau,t,T_0)$). In Sections II and III we have thought of an approach, based on this algorithm where the evolution of the Laplace variables s is studied as a function of time. By analogy with time-frequency analysis, hereafter, this approach will be call Time- Laplace analysis. However, at this point there is still a problem: in practice, how can this method be applied to analyze DLS experiments carried out on non-equilibrium, non-ergodic or non-stationary systems? In this section, we summarize what has already been written in this article and explain how this method is implemented.

A. Concepts of Time-Laplace analysis.

To illustrate our approach and demonstrate that usual DLS approaches cannot work properly for non-stationary systems, we will use a toy example. Let us consider a non-stationary signal measured over 100 s, with an instantaneous relaxation time, $\zeta(t)$, evolving linearly as a function of time from 0.35 s to 1 s throughout its measurement (Fig. 3, left panel). First of all, let us carry out a classical DLS experiment where the ACF is built thanks to a correlator upon an estimation window T_0 (which, in this case, is also the measurement duration ΔT). If $T_0 = 100$ s, then the ACF appeared to be a single decaying exponential function (there is barely a factor 3 in ζ between the starting and ending times), and it returns an average relaxation time (Figure 3, central panel). If $T_0 = 10$ s, it is computed 10 ACFs over 100 s and each ACF returns a relaxation time that depends on t (see right panel of Figure 3); this provides a more realistic view of the real instantaneous relaxation time as this one evolves less on a small window. This simple example clearly shows the importance of T_0 choice to properly analyze a signal, the relaxation times of which evolve as a function of time. However, if nothing is known about the temporal evolution of the relaxation times, which is often the case when performing an experiment, it is very difficult to choose the right estimation window for the correlator. Moreover, additional difficulties arise when several relaxation times are involved. In this example, if a second relaxation time $\zeta_2 = 10$ s is added, it is not possible to measure it using 10 windows. Two issues, indeed, raise from the non-stationarity of the scattering signal:

- Using a correlator, the signal acquisition and its process only allow to take “snapshots" of the dynamics of the system which average the relaxation times. For systems undergoing temporal evolution, it may lead to inaccurate information.

- Furthermore, it is no longer possible to iterate the computation of the ACFs to average them in order to reduce the experimental noise; in other words it is not possible to increase the signal/noise ratio using several data acquisitions.

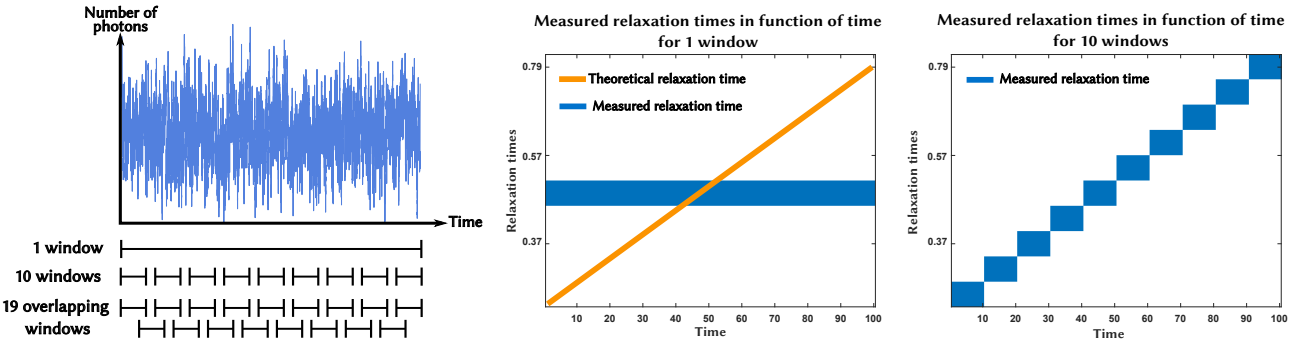

FIG. 3. Scheme illustrating our method: We compare the relaxation time(s) extracted when they are computed i) from only one large temporal window (middle panel) ii) from several shorter windows (right panel).

Therefore, in order to obtain a correct measurement of the temporal evolution of all the relaxation times existing in the system using a correlator, it would be necessary to measure several ACFs with different delays and acquisition durations. Each $g_2(\tau,t,T_0)$ would have to be measured on a different sample which must have the same evolution as the others. This is experimentally complicated and time consuming. It is therefore necessary to find out an alternative.

Consequently, the Time-Laplace method we propose consists in decoupling the data acquisition and their analyzes. Instead of building the scattered intensity ACF using a correlator, we simply record the raw scattered intensity as a function of time, *i.e.* $I_{\text{scat}}(t)$, over a duration ΔT, by means of an acquisition card. In other words, I_{scat} is sampled at a frequency $f_0 = 1/\delta t$ Hz over ΔT seconds. Thanks to this, non-stationary ACFs, $\hat{g}_2(\tau,t,T_0)$, can be estimated according to eq (7); there T_0 and the starting times t at which the ACFs are computed are taken as tunable parameters in post-processing. This avoids preliminary experiments to figure out the relevant relaxation time range to probe. More importantly, it gives the possibility to zoom in or out to focus on specific relaxation time ranges, providing thus a more dynamic view of the time evolution of processes under investigation. This is achieved simply by using short or long T_0; small T_0 to better follow the time evolution of short relaxation times, larger T_0 if the focus is on studying slower relaxation times (note that for a chosen T_0, only the relaxation times s less than about $T_0/10$ are physically relevant, as the larger relaxation times are dominated by estimation problems). The measurement of I_{scat} is performed over a long ΔT, that takes into account the complete dynamics of the studied system. In this way, on a sole experiment and even for out-of-equilibrium systems, it is possible to process the scattering data at different scales of resolution T_0, for all relevant τ and s. The starting times t of ACF computing can be sampled every T_0, yet there is advantage to use oversampling. This later point allows partial overlap between two consecutive windows. If we return to the example, we can sketch 19 windows of $T_0 = 10\,\text{s}$, where the starting time of the n-th window is $t_n = 5(n-1)\,\text{s}$ as sketched on the left panel of Figure 3 (hence overlap between two consecutive windows of 5 s). This provides a more continuous estimation of $\hat{G}(s,t,T_0)$ as a function of t, leading to obtain a "smoother" evolution of the dynamics, without decreasing T_0 (*i.e.* the size of the window over which the ACF is computed). It will even allow us to track abrupt time variations.

Let us summarize the method for the proposed Time-Laplace approach:

- **Time-Laplace parameters:**
  - **Signal acquisition:** Sampling rate of $I_{\text{scat}}(t)$: δt, it is the inverse of the acquisition frequency ($f_0 = 1/\delta t$). Measurement duration: ΔT.
  - **ACF computing:** Window duration: T_0. Number of windows: N_w. Starting times of n-th window: t_n with n between 1 and N_w. Number of points in delays τ_j: N.
  - **ACF analysis:** Number of points in Laplace variable s_k: N_s. Parameter of regularization γ.
- **Input:** $I_{\text{scat}}(t)$ recorded over the duration ΔT.
- **Signal processing:**
  - Split $I_{\text{scat}}(t)$ into N_w sub-signals covering window $[t_n, t_n + T_0]$.
  - For each sub-signal:
    - Compute the ACF of the centered and normalized intensity, eq. (7), and keep the downsampled version at the N points τ_j.
    - Apply ILT algorithm, minimizing eq. (17); it returns: $\hat{G}(s_k,t_n,T_0)$.
- **Output:** 2D-map $\hat{G}(s,t,T_0)$, characterizing temporal evolution of the dynamics of the system.

  In the following, $\hat{G}(s_j,t_n,T_0)$ is displayed as a 2D-map in the time-Laplace domain (t_n,s_k) (like in well-known Time-Frequency methods). The y-axis is the relaxation times s (Laplace domain) and the x-axis the window starting time t at which the ACF is computed; $\hat{G}$ is displayed color-coded with a suitable colormap.

We use the method as described above, with a logarithmic spacing in τ_j and s_k, with overlapping windows of duration T_0 at times t_n so as to follow in a smoother way the temporal evolution of the relaxation times.

B. Light scattering signal acquisition

Let us now describe what is the second key to our approach: the acquisition of the light scattering signal. In practice, the scattered photons are detected by means of an avalanche photodiode (Perkin Elmer) that is a photon counting system capable of detecting single photons of light over visible to near infrared wavelength range (400 nm to 1060 nm). This module is supplied by a triple output stabilized DC Power Supply (BK Precision-BK9130). The maximum number of photons that can be detected is of the order of 10^7 photons/s. Over the visible range the APD module detects about $60-70\,\%$ of the received photons and its "dark noise" is in the range of $150-200$ counts/s, so much lower than the number of photons detected in our experiments (typically of the order of, or larger than 10^5 photons/s). Each photon detected by the photodiodes gives rise to a transistor-transistor logic pulse (TTL). These pulses are sent to a "counting" channel of a data-acquisition card, which allows for counting each detected photon (DAQ NI USB-6361 - National Instrument; resolution 32-bits and maximum acquisition rate 10 MHz). To measure the scattered intensity as a function of time, $I_{\rm scat}(t)$, the number of photons detected by the APD, N_p, is counted during time intervals δt over a duration ΔT that is much larger than δt (δt is the sample time; $\Delta = \nu\delta t$, where ν is the number of times the photon counting process is repeated). Thus, $I_{\rm scat}(t_i) = N_p([t_i, t_i+\delta t_i])$. The acquisition card is computer-controlled by means of a LabVIEW program we developed that provides the number of detected photons as a function of time, $N_p(t)$. Both values of parameters δt and ΔT can be monitored. The choice of both parameters is essential to ensure that the measurements of the scattering intensity upon time provide reliable information on the dynamic properties of the considered sample. Basically, δt has to be short enough to allow access to the entire "fast" dynamics of the system, while ΔT has to be long enough so it can provide access to the full "slow" dynamics of the system. Moreover, to ensure good photon statistics, the incident laser power as to be set so there are at least ten photons in each δt interval are required, with the constraint that the number of photons detected per second is less than 10^7 photons.

V. DLS EXPERIMENTS WITH OUT-OF-EQUILIBRIUM SYSTEMS: EXPERIMENTAL VALIDATION

To experimentally validate the proposed Time-Laplace method, we investigate the time-evolution of the dynamics of three different non-equilibrium processes or systems: the cooling kinetics of a colloidal particle solution; the sol-gel transition; and the internal dynamics of a living cell nucleus.

A. Temporal evolution of particle Brownian motion upon cooling

First of all, we apply the Time-Laplace method to the investigation of the Brownian relaxation of colloidal latex particles in a solution whose temperature evolves spontaneously from $\sim 59^{\rm o}$C to $\sim 19^{\rm o}$C. The temperature relaxation as a function of time induces changes in the particle diffusion coefficient D_0 through the evolution of temperature and viscosity ($D_0 = k_B T/6\pi\eta R_h$). This therefore creates a simple out-of-equilibrium process based on a solution of latex particles and we try to measure $D_0(t)$ throughout the cooling process.

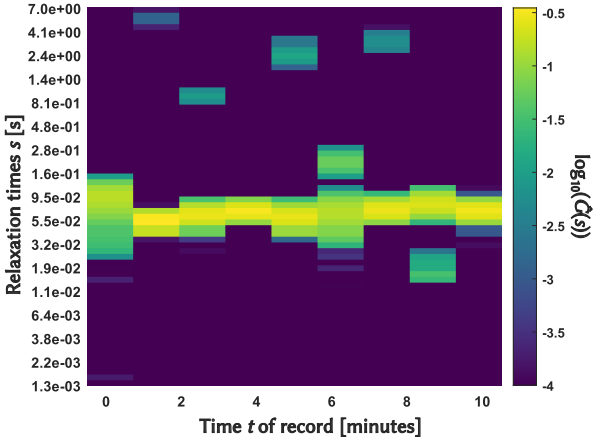

FIG. 4. Density map of the extracted relaxation times from a colloidal solution at constant temperature (paragraph V A 0 a). The x-axis corresponds to the beginning time when the ACF was computed. The y-axis corresponds to the measured relaxation times. The colorbar displays the density of the relaxation times distribution. T_0 = 1 min, overlap = 0%, $\gamma = 1$, signal was recorded for 10 minutes.

The investigated system is made up of 9 g of glycerol, 1 g of water, and 0.1 g of an aqueous solution of spherical latex particles with 1 wt% of solid. This colloidal solution is provided by the Duke Scientific Corporation and used without further purification (indicated particle radius: 100 ± 3 nm). The 0.1 g of this solution is mixed with 1 g of milliQ ultrapure water ($\rho = 18 \pm 0.1$ MΩ cm; from an in house ELGA system). The obtained mixture is filtered through a porous Nylon membrane with pores of 0.45 μm diameter (Millex-HA syringe filter), to remove dusts and aggregates. It is then mixed with 9 g of glycerol. The obtained solution is allowed to equilibrate at room temperature over $\sim$ 24 hours. About 1.5 g of this final solution is placed in a cylindrical glass tube of 8 mm diameter that is set at the center of a vat containing an index-matching liquid (decahydronaphthalene). A thermocouple is inserted into the tube to allow *in situ* measurement of the sample temperature (accuracy $\pm 0.1^{\rm o}$ C). The internal temperature of the vat is monitored thanks to a thermal bath (Lauda); this sets the sample temperature. The sample is irradiated with a laser (Laser Quantum GEM, vertically polarized; $\lambda = 532$ nm), the detector is placed at an angle θ with respect to the direction of the incident beam. For $\lambda = 532$ nm, the refractive index of the sample is ~ 1.45 and its temperature variation is assumed to be negligible. The sample viscosity as a function of temperature is measured using a Kinexus Ultra+ rheometer, with a cone-plane geometry (cone characteristics: $2^{\rm o}$ - 60 mm).

a. Colloidal system at constant temperature. DLS experiments are used to measure the latex particle radius at dif-

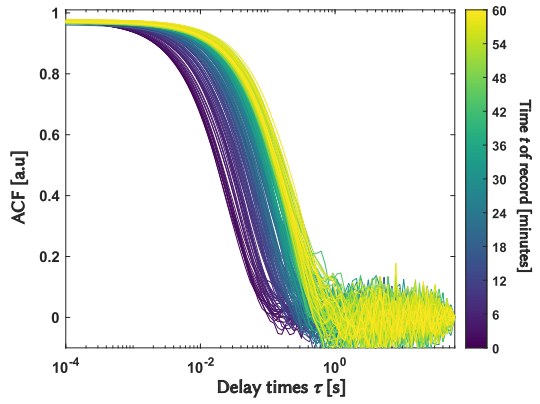

FIG. 5. ACFs computed along the experiment of the relaxation in temperature (paragraph V A 0 b) with T_0 = 60 s, each color corresponds to a computed time indicated by the colorbar.

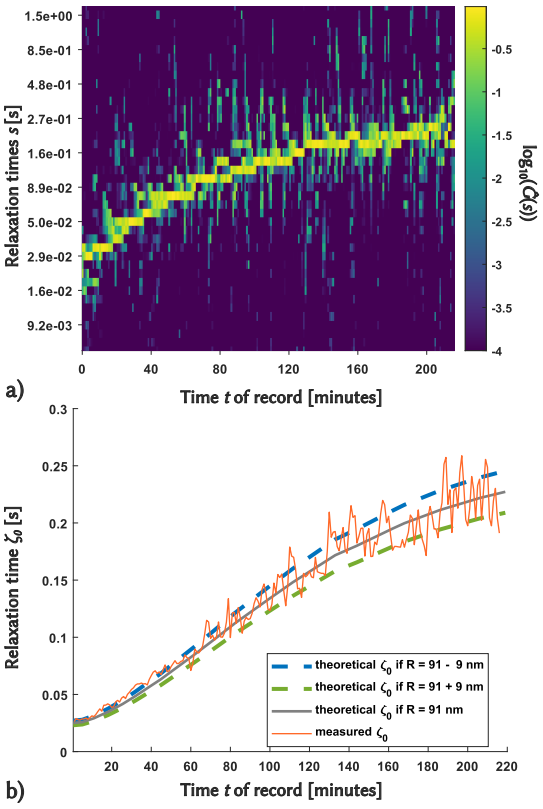

FIG. 6. Visualization of the relaxation times for the temperature relaxation experiment (paragraph V A 0 b). (a) Top panel: Density map of the extracted relaxation times from a colloidal solution when temperature is relaxing. T_0 = 120 s, $\gamma = 1$, overlap = 50%. (b) Bottom panel: Main relaxation time extracted $\zeta_0(t)$ (see eq.20) for each time t (orange curve), expected relaxation time if $R_{\text{mean}} = 91$ nm (gray curve), expected relaxation times if $R_{\text{mean}} = 91 \pm 9$ nm (dotted lines).

ferent temperatures between 19°C and 59°C (*i.e.* 19.6°C, 32.0°C, 41.3°C, 51.2°C, and 58.3°C, respectively). Measurements are performed both by direct estimation of the ACF of the light scattering signal thanks to a TurboCorr Digital Correlator (Brookhaven Instruments), as well as acquiring the scattering intensity I_{scat} as a function of time according to the Time-Laplace procedure described in Sec. IV B (here: $\delta t = 10^{-4}$ s and $\Delta T = 600$ s). Fig. 4 shows the output of a scattering signal recorded over 10 minutes at T=41.3°C and analyzed with our Time-Laplace approach. Here, ACFs are computed over 1 minute sliding windows with no overlap between two consecutive slots. One notices that for most of the windows the analysis does not return a single relaxation time; very likely, because despite our efforts the sample is not simply a dispersion of monodisperse latex beads. However, one of the observed relaxation processes is always seen, its characteristic time does not evolve, and its amplitude is always much higher than that of the others. Moreover, this relaxation time corresponds to that obtained by fitting the ACF with the cumulant model. It is thus assumed that it corresponds to ζ_0 the relaxation time of the Brownian motion of the particles:

$$\zeta_0 = \frac{1}{2D_0 q^2} = \frac{3\pi\eta R_h}{k_B T q^2} \tag{19}$$

Both methods lead to the same result: it is found a particle radius $R_h = 91 \pm 9$ nm, which seems to be rather constant as a function of temperature in the studied range. We use this measured size in the following. These experiments prove that the Time-Laplace method works well when the system under investigation is in thermodynamic equilibrium and so the scattering signal is stationary.

b. Cooling kinetics of a colloidal system. The initial temperature of the sample, T_i, is set to 58.6 ± 0.1°C. We wait for half an hour to make sure that the sample has reached its thermodynamic equilibrium prior to starting the measurement.

- To start with, light scattered by the sample at T_i is recorded for 2 minutes (acquisition with a sample time $\delta t = 10^{-4}$ s).
- Then the thermal bath is turned off. This sets the beginning of the experiment, $t = 0$ s; the system (vat + sample) is let to cool down to room temperature; $T_f = 19 \pm 1$°C. $I_{\text{scat}}(t)$ is recorded during the cooling process until 23.2°C. Parameters of the signal acquisition are: $\delta t = 10^{-4}$ s and $\Delta T = 13\,200$ s (220 minutes). During the whole experiment, temperature inside the sample is read every 30 s.

For this experiment, ACFs are computed from $I_{\text{scat}}(t)$ over 2 minutes sliding windows with an overlap between two consecutive slots of 50 % (i.e. one minute). Figure 5 shows the evolution of the ACFs with time. It is noticed that the decay rate of these ACFs shifts towards large relaxation times as the system cools. The $\hat{G}(s,t)$ distribution is extracted for each ACF; an example of fit is displayed in Fig. 7. The agreement between the experimental ACF and that which can be calculated from the found $\hat{G}(s,t)$ distribution is always very good.

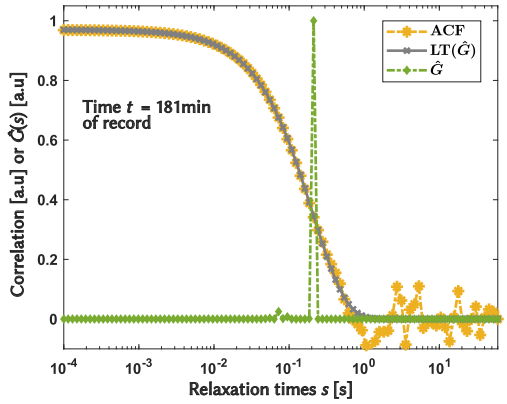

FIG. 7. Visualization of the data adjustment with the proposed ILT algorithm for the temperature cooling experiment. The yellow curve (stars) shows the ACF computed from the data. The ACF was computed 181 min after the beginning of the experiment with T_0 = 60 s. The green curve (diamonds) exhibits the distribution of relaxation times $\hat{G}(s)$ computed with the proposed method with $\gamma = 1$. The gray curve (crosses) is the ACF fit calculated from the result $\hat{G}(s)$ using eq. (14).

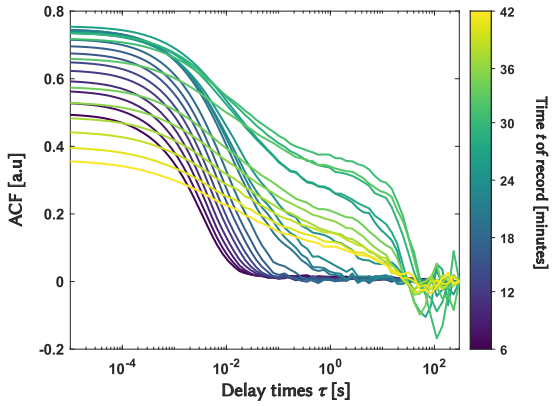

FIG. 8. ACFs computed along the experiment of the transition sol-gel with T_0 = 300 s (paragraph V B).

As expected, it is clearly seen that the sample dynamics slows down with time (see Fig 6 (a)). One notices that in almost all cases, the relaxation is not a single exponential; several relaxation times can be observed. Nevertheless, one relaxation always dominates strongly; its amplitude being much higher than that of the others. The temporal evolution of this relaxation time is assumed to be the evolution of the relaxation time of the Brownian motion of the particles $\zeta_0(t)$ as the system cools down.

The radius of the latex particles is known, as well as $T(t)$ the temperature in the sample as a function time from $t = 0$ s. The sample viscosity as a function of T has been measured. The temporal evolution of the particle diffusion coefficient $D_0(t)$ can therefore be calculated during the cooling process, allowing modeling of $\zeta_0(t)$.

$$\zeta_0(t) = \frac{1}{2D_0(t)q^2} = \frac{3\pi\eta(T(t))R_h}{k_B T(t) q^2} \qquad (20)$$

Fig. 6 (b) displays both measured and calculated values of $s_0(t)$ throughout the sample cooling (with scattering angle $\theta = 45^o$). The agreement between the model and the experiment is good. We conclude that these experiments demonstrate that the Time-Laplace method is suitable to probe the dynamics of systems that are not in thermodynamic equilibrium and when the scattering signal is non-stationary.

Our goal here is to validate the Time-Laplace method and not to investigate what happens in the sample as it cools. Therefore, we will not discuss these results further. However, it is worth noticed that the $\hat{G}(s,t)$ distributions exhibit more relaxation times than those obtained when the sample is in thermodynamic equilibrium. Fluctuations in the measured values of $\zeta_0(t)$ are also observed. We believe these observations come from the non-equilibrium aspect of the phenomenon; cooling induces convection in the sample and as a consequence temperature within the scattering volume may fluctuate significantly in time and space; because of convection, dust or objects larger than the latex beads may pass inside the scattering volume. Therefore, the analysis of the temporal behavior of $\hat{G}(s,t)$ can also provide valuable information on the evolution of the studied system.

B. Sol-gel transition

The second process investigated to test the Time-Laplace method is the sol-gel transition in colloidal solutions. This transition occurs when the repulsive interactions between colloids, which prevent their aggregation, are screened. As a result, colloidal particles can approach close to each other and stick together due to van der Waals forces. It is then observed growth of fractal objects formed by their aggregation[59,60]. Once these structures percolate the gel phase is formed.

Here, the used system is an aqueous solution of silica nanobeads of $\sim$ 12 nm diameter. This colloidal suspension is stabilised due to electrostatic interactions between the particles. In that case, addition of ions to the solution changes the ionic strength and leads to screening of these interactions and induces the transition. Concentration in silica particles, as well as the kind of ions added to the solution and their concentration monitor this transition and its kinetic[61].

For these experiments, we used two different DLS setups; the setup used for the colloid solution cooling experiment as in Sec. V A, and a setup we developed to investigate the dynamics of a living cell nucleus. Here, it is only displayed experiments performed with the latter device. 0.3 g of the final mixture is introduced into a special chamber of $10 \times 10 \times 3$ mm^3, that is made by sandwiching a stainless frame ($65 \times 35 \times 3$ mm^3) between 2 microscope slides. This provides a container of low thickness and small volume whose both sides of entry and exit of light are transparent. The solution is introduced into this chamber thanks to two channels of 1 mm diameter drilled in the section. The chamber is set in a vice, the glass surfaces perpendicular to a laser beam (He-Ne laser, vertically polarized; $\lambda = 632,8$ nm). Temperature

is $\sim 20^{o} \pm 0.5^{o}$C. Once the sample is placed, recording of the scattering signal is started with the following parameters: $\delta t = 10^{-5}$ s and $\Delta T = 2400$ s (40 minutes). These measurements were made at $\theta = 12^{o}; 25^{o}$ and 30^{o}.

Here, it is shown the result of an experiment performed using the second DLS setup, with $\theta = 25^{o}$. The recording of the scattering signal starts 6 minutes after the mixing of the solutions. The colloidal solution is prepared by simply mixing 4.54 g of LUDOX® HS-40 (suspension of colloidal silica in H_2O with 40 wt % of solid; from Sigma Aldrich) with 13.39 g, of milliQ ultrapure water ($\rho = 18 \pm 0.1$ MΩ cm; from an in house ELGA system). In order to remove dusts and big aggregates, the obtained solution is first filtered through a glass fiber membrane (GF/A) with pores of 1.6 μm diameter (Whatman® Puradisc 13 syringe filters). At the same time, 3.93 g of a NaCl solution with a NaCl concentration of 17.55 wt % are prepared. At $t = 0$ s, 0.33 g of the NaCl solution are added to 1.5 g of the colloidal mixture. This gives rise to a final solution with a colloidal silica concentration of 8.3 wt % and a NaCl concentration of 3.15 wt %. Dissociation of NaCl molecules into Na^+ and Cl^- ions make the electrostatic interactions between particles vanish (the negative charges of the silica nanobeads are screened by Na^+ ions) and the gelation process starts. According to rheology studies[62], in these experimental conditions, it takes about 27 minutes after mixing the two solutions to form the gel phase.

Figure 8 shows the evolution of the computed ACFs as a function of time throughout the gelation process (in this case, ACFs are computed from $I_{\text{scat}}(t)$ over $T_0 = 300$ s with an overlap between two consecutive slots of 70 %). The observations are coherent with previous works[59]: First, the value of the ACFs plateau that is seen at short delay times increases (this is related to the increase in scattered intensity), then, in a second part, the plateau position starts to decrease with time (due to the decrease of the scattered intensity). This change of behavior in the scattering intensity is assumed to indicate the full gelation of the sample; the drop of the plateau of the ACFs indicating a reduced mobility due to the formation of a long-range network. According to this result, the full gelation process takes about 26-27 minutes after the mixing, in agreement with rheology measurements. It is also noticed that the shape of these ACFs evolves strongly as gelation process progresses. At the beginning of the process, the ACFs are close to a single exponential decay with a short relaxation time, then the ACFs take on a more and more pronounced stretched exponential shape, with an increasing relaxation time.

Figure 9 shows an instance of the ACF fitted by the proposed method. One sees that (here before full gelation) the distribution of relaxation times is largely spread over two decades. Figure 10 displays four different Time-Laplace analyses of the recorded signal along the full experiment.

- ACFs are computed from $I_{\text{scat}}(t)$ over $T_0 = 5$ s sliding windows with no overlap between two consecutive slots.
- ACFs are computed from $I_{\text{scat}}(t)$ over $T_0 = 60$ s sliding windows with an overlap between two consecutive slots of 70 %.
- ACFs are computed from $I_{\text{scat}}(t)$ over $T_0 = 120$ s sliding windows with an overlap of 70 %.
- ACFs are computed from $I_{\text{scat}}(t)$ over $T_0 = 300$ s sliding windows with an overlap of 70 %.

This figure clearly shows the influence, on the distribution of relaxation times, of the duration T_0 of the window over which the ACFs are computed. However, some characteristics are preserved. In particular the change in dynamics between the gelation phase and the gel phase. During the whole gelation phase, the dynamics evolves as a function of time. Regardless the time at which the scattered signal is analyzed, or the window over which the ACFs are computed, we always observe several relaxation times that are more and more widely distributed as the gelation process progresses. The overall dynamics slows down; the relaxation time with the largest amplitude increases exponentially with time. Once the system has turned into a gel phase, its dynamics changes. The system is non ergodic but does not seem to evolve much with time (at least not over 25 minutes); it is observed several relaxation processes between 10^{-4} s and 10^{-1} s, as well as a very long relaxation time (~ 15 s), which is caught correctly only if the ACFs are computed over a large window ($T_0 = 300$ s). The fact that, in the sample, there are several relaxation times of non-negligible amplitudes, distributed over 2 to 3 decades in time, at the same observation window, most likely explains the observed stretched exponential shape of the ACFs.

Our results are consistent with the results of other groups on similar systems[59,61]. Nevertheless, we believe that the method we have developed and are using (both signal acquisition and Time-Laplace analysis) provides more information on the dynamics of the system during gelation and in the gel phase. Again, the purpose of these experiments is not to precisely study the dynamics of the processes associated with gelation, or that of the gel phase, and therefore, we will not go further in the discussion of our results.

C. Dynamics of a living cell nucleus

In this third example, we use the method to investigate the dynamics inside a living cell nucleus. This experiment is the reason why the method was originally developed (the combination of acquisition and signal processing). The first attempts to study the internal dynamics of a living cell nucleus using dynamic light scattering experiments date back about 10 years ago[33–35]. These first experiments showed that DLS could be useful to study these dynamics. Nonetheless for this approach to be truly effective, an effort was to be done to dispose of a signal processing of the scattering signal that takes into account the fact that a cell nucleus is an out-of-equilibrium system, with a very broad relaxation time distribution.

To perform these experiments, we use the experimental device that has been developed by Suissa *et al.*[33–35] to carry out these first attempts to investigate the internal dynamics of the nucleus of a living cell by means of DLS. The details of this setup are presented in the references[33–35]. A He-Ne laser

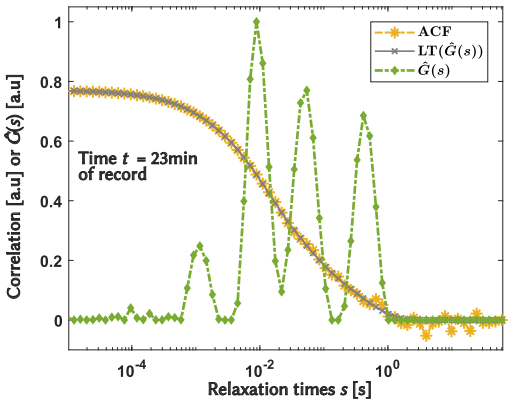

FIG. 9. Visualization of the data adjustment with the developed ILT algorithm for transition sol-gel experiment. The yellow curve (stars) shows the ACF computed from the data. The ACF was computed 23min24 after the beginning of the experiment with T_0 = 60 s. The green curve (diamonds) exhibits the distribution of relaxation times $\hat{G}(s)$ computed with the proposed method with $\gamma = 1$. The gray curve (crosses) is the ACF fit calculated from the result $\hat{G}(s)$ using eq. (14).

beam is focused with a microscope objective (Nikon, magnification 20×, N.A. 0.45) onto a glass surface to which the cells have adhered. Before passing through the microscope objective, the laser beam is enlarged using a beam expander (3×) to obtain a beam waist smaller than the nucleus diameter. The laser beam waist diameter on the surface is then of the order of 3-4 μm, hence less than the nucleus diameter of the investigated cells. In order to enable us to visualize the adherent cells, the objective lens that focuses the laser beam is used to make a bright field transmission microscope. The sample is illuminated with a white light that propagates in the direction opposite the laser beam propagation. The image of the observed field is formed on a CCD camera (JAI CB-080 GE- Stemmer Imaging), thanks to a homemade ocular that provides additional magnification of the order of 1.6× - 1.7×, thus the final magnification of this homemade microscope (objective + "ocular") is of about 34×. By means of this system the adherent cells as well as the reflection spot of the laser beam on the surface can be observed and using translation stages to move the glass surface, the nucleus of one cell can easily be brought into the beam waist. The light scattered by the nucleus is collected at an angle θ which is either 12°; 25° or 30°. For each angle, the image of the scattering volume (*i.e.* the nucleus volume illuminated by the laser beam) is formed on the entrance face of a single mode optical fiber (core diameter: 5 μm, N.A.: 0.6) using a focusing lens of focal length 7.5 cm. This system of collection of the scattered light selects only a part of the nucleus volume that is illuminated; the magnification of the scattered light collection optics is of the order of 1, thus the scattering volume is estimated to be of about 50 μm^3. An interferential filter (central wavelength 630 nm, 10 nm bandpass) is placed right before the optical fiber to avoid polluting the detection of the scattered light with parasitic light.

The experiments were carried out on nuclei of HeLa line living cells[63], in the G1 phase *i.e.* the first stage of the cell cycle). In order to keep the cells alive throughout the experiment duration and avoid any kind of contamination by bacteria and/or yeast, the cells immersed in their culture medium are introduced into the chamber described in the previous section. Prior to the experiment the stainless frame used to make the culture chamber is placed in a surfactant solution for two hours (4% of Decon 90) then brushed before being rinsed with both ultra-purified water (USF Elga) and ethanol. Finally this frame is dried with nitrogen and autoclaved. The 2 microscope slides are cleaned and autoclaved before being stuck on the stainless frame using silicon seals. Once the seals are dry, the cells and their culture medium are introduced into the chamber through the channels drilled in the section of the frame, which are then hermetically sealed so that the chamber inside does not have any contact with the external medium. The chamber is left horizontally in an incubator, at 37°C, for three hours, to let the cells adhere to the bottom glass surface. Then, the chamber is set vertically in a vice, with the glass surfaces perpendicular to the laser beam, the "bottom surface" set further from the objective lens. By means of a heating resistor set in the vise, we assure a temperature control within the culture chamber at $\sim 37^{\circ}$C. The culture medium is made of DMEM (Dubbelco Modified Eagle Medium), supplemented with 10% of foetal calf serum, 1% of L-Glutamine 1M and 2.5% of a 1M Hepes buffer to maintain physiological pH. These culture conditions (culture medium and temperature of about 37°C) allow us to cultivate the cells in these chambers under conditions approaching those of an incubator.

Figure 11 shows a scattering signal recorded as a function of time for the nucleus of a HELA cell in G1 phase ($\delta t = 10^{-5}$ s, $\Delta T = 600$ s). This signal fluctuates a lot, with large and rapid variations of the scattered intensity. Figure 12 displays four different Time-Laplace analyses of this recording signal with:

- $T_0 = 10$ s sliding windows with no overlap;
- $T_0 = 60$ s sliding windows with an overlap of 70%;
- $T_0 = 120$ s sliding windows with an overlap of 70%;
- $T_0 = 300$ s sliding windows with an overlap of 70%.

As in the case of the sol-gel transition, being able to compute ACFs on temporal windows of variable size with an overlap between two consecutive windows that can be changed, allows us to probe the nucleus dynamics between $\sim 10^{-5}$ s and ~ 30 s. It can be seen three different dynamics that are clearly distinct: dynamics with relaxation times between $\sim 10^{-2}$ s and $\sim 4 \times 10^{-2}$ s; dynamics with relaxation times between $\sim 5 \times 10^{-1}$ s and ~ 1.5 s and finally dynamics with relaxation times between ~ 10 s and ~ 30 s. These dynamics do not seem to change much over 10 minutes, however, if the same measurement is repeated one hour later, the two fastest dynamics appear to be different, likely due to a different biological activity within the nucleus.

Our results are consistent with the results of Suissa *et al.*[33–35]. Again, our purpose in this article is not to study the dynamics of a living cell nucleus, and therefore, we will not

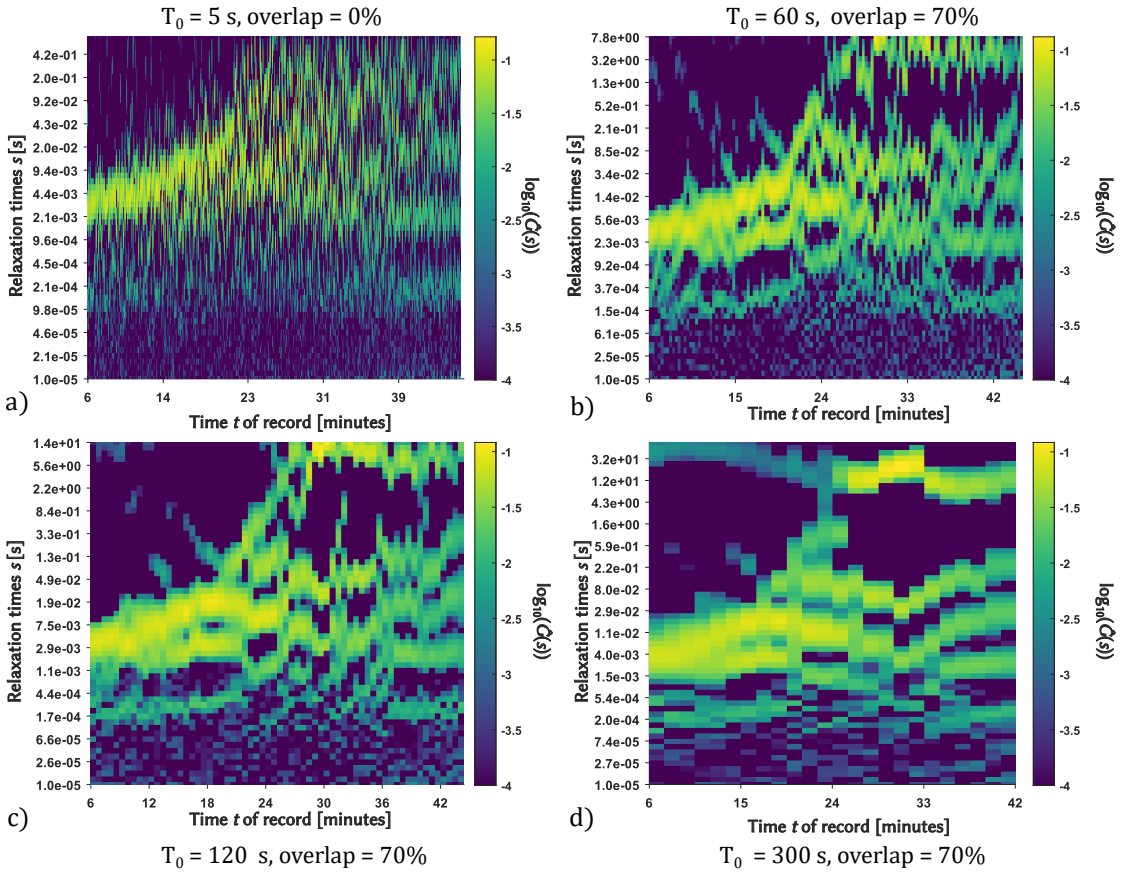

FIG. 10. Density maps of the relaxation times computed with different parameters for the transition sol-gel experiment: a) $T_0 = 5$ s, overlapping rate = 0%, b) $T_0 = 60$ s, overlapping rate = 70%, c) $T_0 = 120$ s, overlapping rate = 70 %, d) $T_0 = 300$ s, overlapping rate = 70 %. On the x-axis: Time t when the ACF has been computed (in minutes), the scale is logarithmic. On the y-axis: Relaxation times s, in seconds, estimated using the developed ILT algorithm, eq. (13); the scale in s is logarithmic. The color represents the density of the relaxation time, the scale is logarithmic. $\gamma = 1$ for the four figures. Signal duration is 40 minutes.

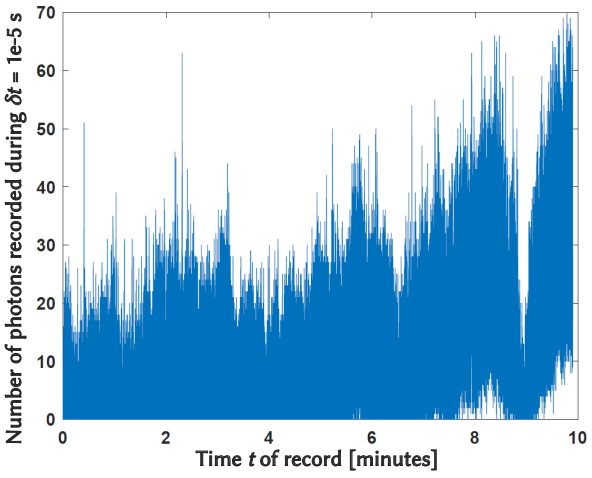

FIG. 11. Light scattering signal from a HeLa cell nucleus in G1 phase. Signal recorded over 10 minutes at $f_0 = 10^5$ Hz.

go further in the discussion of our results. Still, these results prove that we have got the tools (both signal acquisition and Time-Laplace analysis) to investigate the evolution of the dynamics of a living cell nucleus as a function of its biological activity.

VI. CONCLUSION

In this article, we present a new method to analyze DLS signals from out-of-equilibrium systems. This method, we call Time-Laplace analysis, is based on a regularized ILT of sliding ACFs of the scattered signal, computed upon estimation windows that can be modulated. This approach is then multiscale, systematic and more robust than the classical CONTIN algorithm.

Here, we discuss the principles of the method, and we describe the signal processing techniques, as well as the experimental set-up, that we develop in order to use dynamic light scattering in general situations. On different out-of-equilibrium systems, we prove that this method enables us to extract the non-stationary distribution of relaxation times from DLS experiments. The main limitation of this multiscale approach is the necessity to compute the ILT over windows with

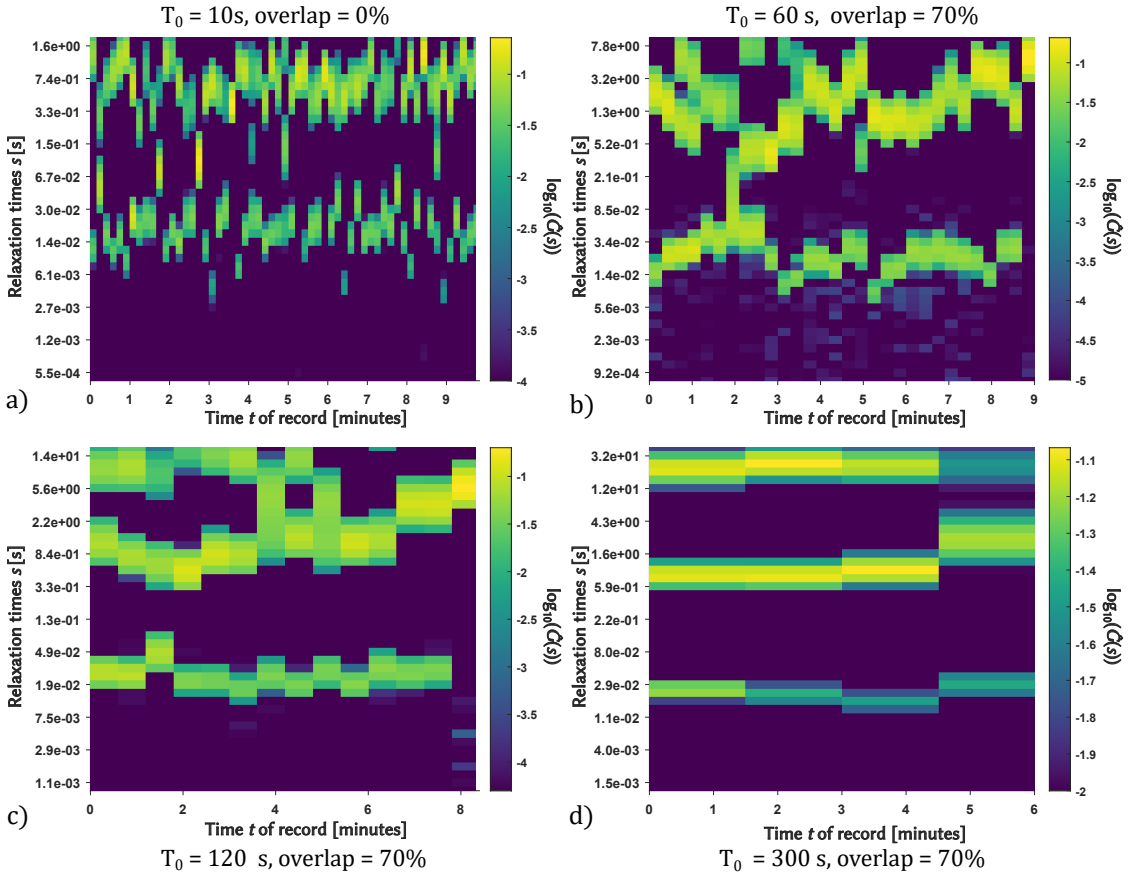

FIG. 12. Density maps of the relaxation times computed with different parameters for the DLS experiment on living Hela cells: a) T_0 = 10 s, overlapping rate = 0%, b) T_0 = 60 s, overlapping rate = 70%, c) T_0 = 120 s, overlapping rate = 70 %, d) T_0 = 300 s, overlapping rate = 70 %. On the x-axis: Time t when the ACF has been computed (in minutes), the scale is logarithmic. On the y-axis: Relaxation times s in seconds computed with the developed ILT, eq. (13), the scale is logarithmic. The color represents the density of the relaxation time, the scale is logarithmic. $\gamma = 1$ for the four figures. Signal duration is 10 minutes.

different time length T_0, even if we think that an all-in-one computation is possible. A minor limitation is the difficulty to treat ACF decays faster than a simple exponential. Nevertheless, a possibility is to use Gaussian transforms as mentioned in the article of Andrew *et al.*[43]

Therefore, we would like to stress out that the obtained results clearly show that DLS experiments capture all the richness and complexity of the dynamics of various processes and systems, and that the Time-Laplace method we have developed allows to extract them. Henceforth, the proposed approach can prove to be very useful for the study of the dynamics of many out-of-equilibrium "soft matter" systems. We claim, indeed, that this signal treatment can be adapted to numerous DLS experiments dealing with non-equilibrium or non-ergodic systems. In our case we aim at applying this method to investigate the internal dynamics of living cell nucleus. Moreover, this Time-Laplace method could be applied as well in XPCS, but also to all ACFs that could reasonably be decomposed as a weighted sum of exponential decays.

Regarding the signal processing aspect, the next step is to use more efficient algorithms to reduce the numerical expensive cost raised by resolution of inverse problems. Furthermore, S. Provencher (more recently Andrew *et al.*[43]) brought the idea[64] in 1996 to find the distribution of relaxation times for stationary systems by solving an inverse problem regarding the decay times and the wave vectors *i.e.* in a 2D-space. In the same spirit, we could imagine figuring out the distribution of relaxation times according to the decay times but also to the times of recording. This 2D-problem would bring a smoother solution that would reduce noise in our distributions.

ACKNOWLEDGMENTS

The authors kindly acknowledge fruitful discussions with Dr.Thibaut Divoux, Dr. Thomas Gibaud, Dr. Sébastien Manneville, Dr. Stéphane Santucci and Dr. Wilbert Smit and thank Sami Lemaire and Dr. Zakia Mokhtari for their help.

DATA AVAILABILITY STATEMENT

Data are available upon request to the corresponding author.

BIBLIOGRAPHY

[1] T. Tadros, R. Izquierdo, J. Esquena, and C. Solans, "Formation and stability of nano-emulsions," Adv. Colloid Interface Sci. **108**, 303–318 (2004).

[2] P. A. Hassan, S. Rana, and G. Verma, "Making sense of brownian motion: Colloid characterization by dynamic light scattering," Langmuir **31**, 3–12 (2015).

[3] S. Bhattacharjee, "Dls and zeta potential - what they are and what they are not?" J Control Release **235**, 337–351 (2016).

[4] F. Nallet, D. Roux, and J. Prost, "Hydrodynamics of lyotropic smectics: a dynamic light scattering study of dilute lamellar phases," J. Phys. France **50**, 3147–3165 (1989).

[5] T. Bellini, N. Clark, and D. Schaefer, "Dynamic light scattering study of nematic and smectic- a liquid crystal ordering in silica aerogel," Phys. Rev. Lett **74**, 2740–2743 (1995).

[6] É. Freyssingeas, D. Roux, and F. Nallet, "Quasi-elastic light scattering study of highly swollen lamellar and sponge phases," J.Phys. II **7**, 913–929 (1997).

[7] M. Majumdar, P. Salamon, A. Jakli, J. T. Gleeson, and S. Sprunt, "Elastic constants and orientational viscosities of a bent-core nematic liquid crystal," Phys. Rev. E **83** (2011), 10.1103/PhysRevE.83.031701.

[8] S. Zhou, K. Neupane, Y. A. Nastishin, A. R. Baldwin, S. V. Shiyanovskii, O. D. Lavrentovich, and S. Sprunt, "Elasticity, viscosity, and orientational fluctuations of a lyotropic chromonic nematic liquid crystal disodium cromoglycate," Soft Matter **10**, 6571–6581 (2014).

[9] W. Poon, "The physics of a model colloid-polymer mixture," J. Condens Matter Phys. **14**, R859–R880 (2002).

[10] T. Phenrat, N. Saleh, K. Sirk, R. D. Tilton, and G. V. Lowry, "Aggregation and sedimentation of aqueous nanoscale zerovalent iron dispersions," Environ. Sci. Technol. **41**, 284–290 (2007).

[11] D. Saha, R. Bandyopadhyay, and Y. M. Joshi, "Dynamic light scattering study and dlvo analysis of physicochemical interactions in colloidal suspensions of charged disks," Langmuir **31**, 3012–3020 (2015).

[12] S. Brunetti, D. Roux, A. M. Bellocq, G. Fourche, and P. Bothorel, "Micellar interactions in water-in-oil microemulsion. 2. light scattering determination of the second virial coefficient," J. Phys. Chem. **87**, 1028–1034 (1983).

[13] H. B. Bohidar and M. Behboudnia, "Characterization of reverse micelles by dynamic light scattering," Colloids Surf, A Physicochem Eng Asp **178**, 313–323 (2001).

[14] R. Ganguly and N. Choudhury, "nvestigating the evolution of the phase behavior of aot-based w/o microemulsions in dodecane as a function of droplet volume fraction," J. Colloid Interface Sci. **372**, 45–51 (2012).

[15] K. Devanand and J. Selser, "Asymptotic behavior and long-range interactions in aqueous solutions of poly(ethylene oxide)," Macromolecules **24**, 5943–5947 (1991).

[16] W. Brown, F. J, and M. D. Miguel, "Poly(ethylene oxide)-sodium dodecyl sulfate interactions studied using static and dynamic light scattering," Macromolecules **25**, 7192–7198 (1992).

[17] J. Jansson, K. Schillen, G. Olofsson, R. da Silva, and W. Loh, "The interaction between peo-ppo-peo triblock copolymers and ionic surfactants in aqueous solution studied using light scattering and calorimetry," J. Phys.Chem. B **108**, 82–92 (2004).

[18] H. Oguzlu and Y. Boluk, "Interactions between cellulose nanocrystals and anionic and neutral polymers in aqueous solutions," Cellulose **24**, 131–146 (2017).

[19] A. Cumming, P. Wiltzius, F. Bates, and J. Rosedale, "Light-scattering experiments on phase-separation dynamics in binary fluid mixture," Phys. Rev. A **45**, 885–897 (1992).

[20] J.-F. Lutz, K. Weichenhan, O. Akdemir, and A. Hoth, "About the phase transitions in aqueous solutions of thermoresponsive copolymers and hydrogels based on 2-(2-methoxyethoxy)ethyl methacrylate and oligo(ethylene glycol) methacrylate," Macromolecules **40**, 2503–2508 (2007).

[21] W. Poon, A. Pirie, and P. Pusey, "Gelation in colloid-polymer mixtures," Faraday Discuss. **101**, 65–76 (1995).

[22] E. Freyssingeas, M. Graca, S. Wieczorek, and R. Holyst, "Relaxation processes in mixtures of liquid crystals and polymers near phase boundaries and during phase separation," J. Chem. Phys. **120**, 8277–8282 (2004).

[23] S. Manley, H. Wyss, K. Miyazaki, J. Conrad, V. Trappe, L. Kaufman, D. Reichman, and D. Weitz, "Glasslike arrest in spinodal decomposition as a route to colloidal gelation," Phys. Rev. Lett. **95** (2005), 10.1103/PhysRevLett.95.238302.

[24] M. Shibayama and T. Tanaka, "Volume phase transition and related phenomena of polymer gels," Adv Polym Sci **109**, 1–62 (1993).

[25] A. H. Krall and D. A. Weitz, "Internal dynamics and elasticity of fractal colloidal gels," Phys. Rev. Lett **80**, 778–781 (1998).

[26] M. Shibayama, "Spatial inhomogeneity and dynamic fluctuations of polymer gels," Macromol. Chem. Phys. **199**, 1–30 (1998).

[27] M. Laurati, G. Petekidis, N. Koumakis, F. Cardinaux, A. B. Schofield, J. M. Brader, M. Fuchs, and S. U. Egelhaaf, "Structure, dynamics, and rheology of colloid-polymer mixtures: From liquids to gels," J. Chem Phys **130** (2009), 10.1063/1.3103889.

[28] D. Larobina and L. Cipelletti, "Hierarchical cross-linking in physical alginate gels: a rheological and dynamic light scattering investigation," Soft Matter **9**, 10005–10015 (2013).

[29] V. W. van Megen and S. M. Underwood, "Glass transition in colloidal hard spheres: Measurement and mode-coupling-theory analysis of the coherent intermediate scattering function," Phys. Rev. E **49**, 4206–4220 (1994).

[30] L. Cipelletti and L. Ramos, "Slow dynamics in glassy soft matter," J. Condens. Matter Phys. **17**, R253–R285 (2005).

[31] G. L. Hunter and E. R. Weeks, "The physics of the colloidal glass transition," Rep. Prog. Phys. **75** (2012), 10.1088/0034-4885/75/6/066501.

[32] P. J. Lu and D. A. Weitz, "Colloidal particles: Crystals, glasses, and gels," in *ANNUAL REVIEW OF CONDENSED MATTER PHYSICS, VOL 4*, Annual Review of Condensed Matter Physics, Vol. 4, edited by J. Langer (2013) pp. 217–233.

[33] M. Suissa, C. Place, E. Goillot, B. Berge, and E. Freyssingeas, "Dynamic light scattering as an investigating tool to study the global internal dynamics of a living cell nucleus," EPL **78** (2007), 10.1209/0295-5075/78/38005.

[34] M. Suissa, C. Place, E. Goillot, and E. Freyssingeas, "Internal dynamics of a living cell nucleus investigated by dynamic light scattering," Eur Phys J E Soft Matter **26**, 435–48 (2008).

[35] M. Suissa, C. Place, E. Goillot, and E. Freyssingeas, "Evolution of the global internal dynamics of a living cell nucleus during interphase," Biophys. J. **97**, 453–461 (2009).

[36] S. W. Provencher, "A constrained regularization method for inverting data represented by linear algebraic or integral equations," Computer Physics Communications **27**, 213–227 (1982).

[37] S. W. Provencher, "Contin: A general purpose constrained regularization program for inverting noisy linear algebraic and integral equations," Computer Physics Communications **27**, 229–242 (1982).

[38] R. P. Bruce J. Berne, *Dynamic Light Scattering: With Applications to Chemistry, Biology, and Physics*, 2nd ed. (Dover Publications Inc., Mineola N.Y., 2000).

[39] R. J. T. Peter N Pusey, "Particle interactions," in *Dynamic Light Scattering. Applications of Photons Correlation Spectroscopy*, edited by B. J. Berne (Plenum Press, New York, 1985) pp. 85–179.

[40] D. E. Koppel, "Analysis of macromolecular polydispersity in intensity correlation spectroscopy: The method of cumulants," J. Chem. Phys. **57**, 4814–4820 (1972), https://doi.org/10.1063/1.1678153.

[41] B. J. Frisken, "Revisiting the method of cumulants for the analysis of dynamic light-scattering data," Appl. Opt. **40**, 4087–4091 (2001).

[42] A. G. Mailer, P. S. Clegg, and P. N. Pusey, "Particle sizing by dynamic light scattering: non-linear cumulant analysis," J. Condens. Matter Phys. **27**, 145102 (2015).

[43] R. N. Andrews, S. Narayanan, F. Zhang, I. Kuzmenko, and J. Ilavsky, "Inverse transformation: unleashing spatially heterogeneous dynamics with an alternative approach to xpcs data analysis," J. Appl. Cryst. **51**, 35–46 (2018).

[44] R. N. Andrews, S. Narayanan, F. Zhang, I. Kuzmenko, and J. Ilavsky, "Contin xpcs: software for inverse transform analysis of x-ray photon correlation spectroscopy dynamics," J. Appl. Cryst. **51**, 201–205 (2018).

[45] A. G. Zilman and R. Granek, "Undulations and dynamic structure factor of membranes," Phys. Rev. Lett. **77**, 4788–4791 (1996).

[46] A. Madsen, R. L. Leheny, H. Guo, M. Sprung, and O. Czakkel, "Beyond simple exponential correlation functions and equilibrium dynamics in x-ray photon correlation spectroscopy," New J. Phys. **12**, 055001 (2010).

[47] A. K. Livesey, P. Licinio, and M. Delaye, "Maximum entropy analysis of quasielastic light scattering from colloidal dispersions," J. Chem. Phys. **84**, 5102–5107 (1986), https://doi.org/10.1063/1.450663.

[48] Y. Sun and J. G. Walker, "Maximum likelihood data inversion for photon correlation spectroscopy," Measurement Science and Technology **19**, 115302 (2008).

[49] X. Zhu, J. Shen, W. Liu, X. Sun, and Y. Wang, "Nonnegative least-squares truncated singular value decomposition to particle size distribution inversion from dynamic light scattering data," Appl. Opt. **49**, 6591–6596 (2010).

[50] L. Cipelletti, H. Bissig, V. Trappe, P. Ballesta, and S. Mazoyer, "Time-resolved correlation: a new tool for studying temporally heterogeneous dynamics," J. Condens. Matter Phys. **15**, S257–S262 (2002).

[51] A. Duri, H. Bissig, V. Trappe, and L. Cipelletti, "Time-resolved-correlation measurements of temporally heterogeneous dynamics," Phys. Rev. E **72**, 051401 (2005).

[52] A. Fluerasu, M. Sutton, and E. M. Dufresne, "X-ray intensity fluctuation spectroscopy studies on phase-ordering systems," Phys. Rev. Lett. **94**, 055501 (2005).

[53] K. Ludwig, F. Livet, F. Bley, J.-P. Simon, R. Caudron, D. Le Bolloc'h, and A. Moussaid, "X-ray intensity fluctuation spectroscopy studies of ordering kinetics in a cu-pd alloy," Phys. Rev. B **72**, 144201 (2005).

[54] O. Bikondoa, "On the use of two-time correlation functions for x-ray photon correlation spectroscopy data analysis," J. Appl. Cryst. **50**, 357–368 (2017).

[55] A. Fluerasu, A. Moussaïd, A. Madsen, and A. Schofield, "Slow dynamics and aging in colloidal gels studied by x-ray photon correlation spectroscopy," Phys. Rev. E **76**, 010401 (2007).

[56] L. Cipelletti, L. Ramos, S. Manley, E. Pitard, D. A. Weitz, E. E. Pashkovski, and M. Johansson, "Universal non-diffusive slow dynamics in aging soft matter," Faraday Discuss. **123**, 237–251 (2003).

[57] A. Papoulis, *Signal Analysis* (Dover Publications Inc., 1977).

[58] I.-G. Marino, "RILT procedure in MATLAB," https://www.mathworks.com/matlabcentral/fileexchange/6523-rilt (2007).

[59] X. J. Cao, H. Z. Cummins, and J. F. Morris, "Structural and rheological evolution of silica nanoparticle gels," Soft Matter **6**, 5425–5433 (2010).

[60] M. Kawaguchi, "Dispersion stability and rheological properties of silica suspensions in aqueous solutions," Adv. Colloid Interface Sci. **284** (2020), 10.1016/j.cis.2020.102248.

[61] A. S. Zackrisson, A. Martinelli, A. Matic, and J. Bergenholtz, "Concentration effects on irreversible colloid cluster aggregation and gelation of silica dispersions," J. Colloid Interface Sci. **301**, 137–144 (2006).

[62] W. Smit, T. Divoux, and M. Manneville, Result not yet published.

[63] Immortal cell line used in scientific research. It is the oldest and most commonly used human cell line. This line derived from cervical cancer cells.

[64] S. W. Provencher and P. Stêpánek, "Global analysis of dynamic light scattering autocorrelation functions," Particle & Particle Systems Characterization **13**, 291–294 (1996), https://onlinelibrary.wiley.com/doi/pdf/10.1002/ppsc.19960130507.